Applied Thermal Engineering 221 (2023) 119822

Contents lists available at ScienceDirect

Applied Thermal Engineering

journal homepage: www.elsevier.com/locate/ate

Research Paper

Numerical assessment of integrated thermal management systems in electrified powertrains

Alberto Broatch [a], Pablo Olmeda [a,*], Benjamín Plá [a], Amin Dreif [a], Angelo Onorati [b], Andrea Marinoni [b]

[a] CMT-Motores Térmicos, Universitat Politècnica de València, Camino de Vera s/n. 46022 València, Spain
[b] Department of Energy, Politecnico di Milano, Via Lambruschini 4A, 20156 Milano, Italy

ARTICLE INFO

Keywords:
1D modelling
Heat transfer
Hydraulic circuits
Thermal management strategy
Hybrid vehicles

ABSTRACT

Temperatures in internal combustion engines (ICE) impact fuel consumption and pollutant emissions, especially under transient operating conditions. In hybrid powertrains, where the reciprocating internal combustion engine has intermittent operating conditions, a optimum control of these temperatures is critical. In this work, a detailed methodology for studying integrated thermal management systems for hybrid propulsion system was presented. Both experimental measurements and 0D/1D models were implemented and validated for the different components of the hybrid vehicle powertrain. The novelty of this work consists in the extensive experimental measurements involved for the development of the different models, specially the ICE, in order to study the integration of the different thermal flows of a hybrid powertrain. Furthermore, the simulation methodology used in this work integrates different modelling tools and takes advantage of their strengths when compared to using a single modelling tool. Two different thermal management systems have been evaluated under different Real Driving Emission (RDE) cycles at two different temperatures (at 20 °C and -20 °C). Results have shown that during the ICE warming up, the integrated thermal management system improved energy consumption by 1.74% and 3% for warm and cold conditions, respectively. This was because, the integrated TMS allows to avoid the temperature drop of the ICE when the propulsive system is in pure electric mode.

1. Introduction

In view of the current socio-political restrictions and market demands, automotive manufacturers are investing a large amount of resources in research and development (R&D) to further develop innovative power-trains in order to improve their efficiency and reduce their environmental impact [1]. Vehicle electrification has proven to be a promising solution for achieving that aim [2]. In fact, several governments have dictated policies encouraging the shift towards electrified power-trains [3]. Investigations have demonstrated that the hybrid propulsive systems can reduce exhaust emissions and improve fuel economy compared to the traditional propulsive systems based on the internal combustion engine (ICE) [4]. Nevertheless, increasing the rate of vehicle electrification traduces in more expensive vehicles because of the battery and power electronics cost [3]. Overall, electrified vehicles (xEVs) are considered as an important part of the future transportation as a substitute for internal combustion engine vehicles (ICEVs). Although the battery electric vehicles (BEVs) have higher price, they have shown to be competitive and can be expected to be more prevalent in the market due to several attractive features, such as higher energy efficiency, lower maintenance frequency, faster acceleration, and noiseless and emission-free operation [5]. However, BEVs suffer from some obstacles, such as weight, higher cost, limited driving range, extra recharging time and overloaded batteries. Thus, hybrid electric vehicles (HEVs) or plug-in hybrid electric vehicles (PHEV), combining an internal combustion engine (ICE) with an electric motor, have been widely developed because they combine the merits of BEVs and ICEVs. Compared with ICEVs, HEVs can consume less fossil fuel and generate lower Green House Gas (GHG) emissions; while compared with BEVs, HEVs avoid range anxiety due to the power support from ICEs and self-charging batteries. Furthermore, PHEVs can be directly charged from the grid increasing their electric mobility and diminishing the ICE dependence [6].

Thermal management (TM) is critical for maintaining the HEV subsystems temperature within optimum range. In the ICE, the thermal management system (TMS) is responsible for avoiding the failure of the engine material while maintaining the coolant temperature within optimum range for reducing fuel consumption and pollutant emissions.

* Corresponding author.
E-mail address: pabolgon@mot.upv.es (P. Olmeda).

https://doi.org/10.1016/j.applthermaleng.2022.119822
Received 12 July 2022; Received in revised form 16 November 2022; Accepted 5 December 2022
Available online 13 December 2022

Nomenclature

Δt	Time step
Δx	Local mesh size
U	Gas velocity
m	Mass
c	Solid heat capacity
k	Thermal conductivity
A	Area between solid nodes
T	Temperature
$\dot{Q}$	Heat exchanged or generated
d	Distance
h	Convection heat transfer coefficient
c_p	Fluid heat capacity
$\dot{m}$	Flow mass
$[T]$	Array of nodes temperature
$[K]$	Thermal conductances matrix
$[C]$	Capacitances matrix
R_2	Quadratic coefficient of the hydraulic resistance
R_1	Linear coefficient of the hydraulic resistance
R_0	Independent coefficient of the hydraulic resistance
$\dot{V}$	Volumetric flow mass
m_{fv}	The mass of the fluid volume
K_{fa}	Equivalent heat conductance between fluid and ambient
I	Is the cell electric current
E_o	Open circuit voltage
V	Cell voltage
ΔP	Total pressure drop
K	Hydraulic resistance coefficient
$\dot{m}$	Mass flow rate
V	Nominal voltage of the battery pack
P	Power
N	Speed

Acronyms

ICE	Internal combustion engines
0D/1D/3D	0/1/3 dimensional
RDE	Real driving emission
TMS	Thermal management system
xEVs	Electrified vehicles
ICEVs	Internal combustion engine vehicles
BEVs	Battery electric vehicles
HEVs	Hybrid electric vehicles
PHEV	Plug-in hybrid electric vehicles
GHG	Green house gas
TM	Thermal management
BTMS	Battery thermal management system
HVAC	Heating, ventilating and air conditioning
EDS	Electric drive system
EDTMS	Electric drive thermal management system
ITMS	Integrated thermal management systems
OEMs	Original equipment manufacturers
FMI	Functional mock-up interface
EMS	Energy management system
VEMOD	Virtual engine model
CG-TVD	Corberán-Gascón total variation diminishing
CFL	Courant–Friedrichs–Lewy
CPU	Central processing unit
GDI	Gasoline direct injection
PID	Proportional integral derivative
FSM	Fast simulation method
NTU	Number transferred units
ECU	Electronic control unit
ECEM	Equivalent circuit electric model
CFD	Computational fluid dynamic
HX	Heat exchanger
BMEP	Break mean effective pressure
ODE	Ordinary differential equation
IVC	Intake valve closing
EVO	Exhaust valve opening
CAC	Charge air cooling
SI	Spark ignition

Greek symbols

υ	Speed of sound
η	Efficiency

Subscript

i, j	Solid nodes
t	Current time
$t + \Delta t$	Next time step
l	Liquid node
g	Gas node
n	Nodes number
amb	Ambient
$cell$	Battery cell
req	Required

Superscript

i	Solid node
bc	Boundary conditions

Several investigations regarding the improvement of ICE thermal management have been carried out. Split cooling of the cylinder head and liner has been studied by means of a mathematical model [7]. Additionally, in order to reduce the heat rejected to the coolant and increase engine efficiency while reducing emissions, the insulation of engine exhaust ports and manifold was investigated through experimental measurements and numerical tools in different conditions [8,9]. Results showed that fuel consumption could be decreased up to 0.6% while turbine outlet gas enthalpy and pollutant emissions improved by 12% and 30%, respectively. Furthermore, aiming to increase the heat transfer between the cylinder material and the coolant while decreasing the auxiliary coolant pump power, research on nanofluids [10] have been performed. However, although the heat transfer was enhanced, limited fuel saving were observed in the study for transient cycles.

In regard to the battery performance, the battery thermal management system (BTMS) plays a critical role. In fact, the operating temperature of Li-ion battery directly impacts its total capacity, maximum power and durability. Additionally, overheated cells of the battery pack could led to a thermal runaway and failure [11]. According to literature, optimum temperature range of the battery is between 15 °C and 35 °C. Consequently, several investigations have been performed in

order to develop efficient BTMS that maintain the cells temperature of the battery within the optimum range while decreasing the gradient temperature in the battery pack. The BTMS can be classified into different categories depending on type of cooling contact (direct or indirect), phase state of coolant (gas, liquid or phase change material) or its integration with the heating, ventilating and air conditioning (HVAC) system. Additionally, there are novel BTMS based on the use of heat pipes or thermoelectric technology [12]. Another emerging technologies are spray cooling, immersion cooling, and flow boiling cooling [13–15].

The electric drive system (EDS) of an HEV is responsible for the energy conversion between electrical and mechanical power and it consists on an inverter and a electric machine. On one hand, this system works as a motor when consuming energy from the battery in order to drive the wheels. On the other hand, as a generator when charging the battery using the energy provided by the ICE or the regenerative braking. The energy used by the EDS is divided into brake power and power loss generated in the winding, iron, magnet and bearings [16]. This leads to an increment in the temperature of EDS components and, if the material limits are reached, produce a demagnetization of the magnet and/or the windings failure [17]. Thus, efficient TMS in the electric drives are essential for minimizing the temperature of their hotspots. The TMS for the EDS cooling depends on the structural scheme of the electric machine and the performance of the cooling jacket [16]. Several cooling techniques have been studied and implemented in the electric drive thermal management system (EDTMS). Liquid cooling using water and glicol through the jacket, oil spraying for cooling the magnets, forced air cooling, direct water cooling, alternative cooling fluids, immersion cooling, heat pipes, phase change materials, vapour compression refrigeration, thermoelectric cooling and Stirling cycle cooling [16].

Taking into account the diversity of the integrated thermal management systems (ITMS) used by the automotive original equipment manufacturers (OEMs) in their vehicles, it is very clear that an optimum solution is still far from being achieved. Additionally, the different available architectures in xEVs along with their multitude subcomponents make very difficult to find a perfect solution for the vehicle TMS. Each component of HEVs have different thermal requirements. Normally, after the refrigerant loop of the air conditioning system, the cooling loop of the battery has the lowest temperature among the cooling circuits of the vehicle. Some degrees higher, the operative temperature range of the power electronics ranges between 50 °C and 70 °C. Finally, for the ICE, optimum operative temperature is considered to be around 90 °C [2]. Consequently, the ITMS has to be able work in different temperature levels. Thus, the automotive industry presents a diverse level on thermal integration. For the case of BEV, BMW has combined the cooling and heating of the battery with the air conditioning in their BMW i3 (2014) model. Additionally, it has another TMS for cooling the powertrain. The model Tesla S 60 (2013) holds one of the most holistic TMS of the market coupling the cooling of the power electronics, electric machine and battery. Similarly to the BMW i3, the Nissan LEAF (2017) integrates a holistic TMS for the powertrain through active liquid cooling. For its battery, passive air cooling was selected [18].

Numerical tools have become essential for improving the design, developing and testing processes of electrified vehicles. Reducing time to market and obtaining a more optimized solution. However, in most of the cases, specific software or applications are used for modelling each component or subsystem being unable to evaluate the impact of the solution from a holistic perspective [2]. Two different approaches can be taken to avoid this issue. On one hand, benefiting from the extended libraries of some commercial software, modelling every component of the system with the same platform is a possible solution [19–21]. However, this option presents two main drawbacks. Firstly, modelling accuracy is forfeited given the fact that some applications were constructed from the begging aiming to the improvement of a specific subsystem or component. Additionally, several improvements have been implemented in those applications during the last years. Secondly, in larger projects (as it is the case of EVs development), different departments are involved in the process. Each one being specialized in a certain modelling software. On the other hand, a more sophisticated solution, it is to integrate a standardized co-simulation interface. This approach benefits from the accuracy of each specific tool and enables to perform a holistic system simulation. The Functional Mock-Up Interface (FMI) has became commonly used in several simulation tools [22] during the last years.

In this framework, several investigations have been carried out. P. Lu et al. implemented an integrated thermal management system by means of 1D/3D coupling. They modelled the engine cooling circuit, air conditioning and the vehicle under-hood [23]. However, the engine gas circuit was not considered and possible fuel saving were not evaluated. Casoli et al. presented the coupling of ICE, hydraulic circuits in order to develop control models using both Simulink and AMESim simulation platforms [24]. Although the study proved the integration tools potential, only steady-state conditions were evaluated for a conventional engine. R. Yuan et al. published a detailed review on the state of the art of numerical approaches for the virtual holistic thermal and energy management of hybrid vehicles. The investigations showed that great effort had been invested in studying the thermal management of the hybrid vehicle mainly focusing on the battery [2,25]. M. Cao et al. reported a design of an integrated cooling system using Matlab/Simulink along with in-house tools for thermal control development [26]. Although the proposed TMS considered different temperature levels for the HEV subcomponents, the components efficiency was not evaluated. G. Lang et al. presented a study of a cooling circuit layout based on three different circuits and simulated the system for different ambient and load conditions [27]. However, the thermal integration between different cooling circuits and their impact on fuel savings was not evaluated.

Several ITMS have been studied for BEVS [28,29]. However, the integrated thermal modelling with co-simulation approach still needs further exploration and development for hybrid powertrains [30]. J. Ma developed a novel vehicle integrated thermal management system for pure electric vehicles and validated the system through simulation and experimental measurements [31]. S. Hemmati et al. developed a novel model-based optimization platform for the optimal cabin heating operation of a PHEV with engine-assisted heating for cold climate and explored an integrated operation of cabin heating, engine, and aftertreatment for connected PHEVs during real-world drive cycles. However, they used a simplified control oriented ICE thermal model for the ICE and a few effort was invested in developing a model capable of capturing the ICE dynamics, thermal behaviour and fuel consumption during transient operation [32]. M. Shams-Zahraei implemented a new EMS incorporating an engine thermal management based on dynamic programming-based algorithm. Although the control strategy contributed the fuel consumption savings, the implemented TMS only considered the interaction between the thermal flows of the ICE, Cabin and Battery while EDS worked independently [33].

The main novelties in this study are; (a) The extensive experimental campaign carried out in an ICE designed for hybrid propulsion systems. These data guaranteed the correct development, calibration and validation of the submodels implemented. (b) The co-simulation FMI was implemented for different 0D/1D high-fidelity submodels of the ICE, the thermohydraulic and the battery models. Hence, benefiting from the simulation strengths of established modelling tools (i.e. GASDYN and VEMOD) [34,35]. (c) The design methodology of the integrated thermal management system considered the ICE engine cooling circuit layout of a real engine as baseline. Then, the integration of the Battery and EDS cooling systems were integrated while reducing the system complexity and fulfilling temperature requirements.

The main objective of this work is to assess the degree of interaction of the heat flows of an hybrid powertrain system in order to

evaluate the viability of integrated concepts of thermal management systems. For this, the coupling of the ICE, battery, EDS and thermo-hydraulic models was performed. Each component submodel has been constructed in a specialized software and interconnected by means of standardized co-simulation interface. Then, using the available experimental data, the validation of the coupling between the ICE submodels was carried out for different real driving emissions cycles. Additionally, in-house models were developed for the main electric components for estimating the heat rejected to the integrated thermal management system. These were validated with data available in literature. Once the models coupling was completed, two different thermal management systems were developed and simulated for different ambient conditions during an RDE cycle. Finally, the gain in fuel consumption and temperature operation of the different components was evaluated for both considered thermal management systems.

The present paper is divided as follows. First, it starts justifying the importance of the integrated thermal management system on electrified vehicles as well as present the most relevant studies in the field. Second, the numerical models development and coupling is detailed. Third, the experimental set up and the tests are described. Then, the calibration and validation of the different models are presented. Afterwards, the simulation results are presented and analysed. Finally, the most relevant conclusions are stated and explained.

2. Numerical models

The numerical models implemented in this work have been developed in different software platforms (GASDYN software [34], VEMOD (Virtual Engine Model) software [36] and Microsoft Visual Studio).

Note that the purpose of this work was not to simply link already existing models. The ICE submodels were completely constructed, characterized and optimized in this work. The battery model was also developed and validated within the scope of this work while using experimentally characterized parameters data from literature. Furthermore, code development was also required for the improvements of the available modelling tools.

It is important to state the capacities and precision expected from the surrogate models. It is well known that increasing the detail and precision of the models translates in more simulation time. The developed models of this research aim to simulation times close to real time. Thus, although 3D simulations are used for validation, each one of the numerical submodels are based on 0D/1D modelling approach in order to reduce computational effort.

The developed models present different complexity degrees. The ICE models for gas-dynamics, thermo-hydraulics and heat exchange are much more complex than those applied for EDS and Battery, that are based on efficiency maps or first order ODE. This approach was justified because a higher degree of accuracy was required for ICE since more energy was demanded from this component during the RDE cycles. The ICE average energy demand was around 75% of the total for the different tests. Furthermore, the electric motors have relatively higher efficiencies when compared to the engine and their efficiency dependence with temperature is limited while working within safe temperature ranges [37]. The ODE battery model presented acceptable accuracy in previous studies as it can be observed in [38]. Additionally, the temperature variation of the battery is much lower than the one produced in the ICE.

The approach followed in this study searched developing an ITMS which could benefit from thermal flows interaction as simple as possible while fulfilling the thermal requirements of the main components of the hybrid propulsive system. Given the numerous subcomponents of a hybrid vehicle, several combinations and configurations are possible when constructing an ITMS. The HVAC system was assumed to work independently for both thermal strategies evaluated in this work. Hence, zero heat exchange from the ICE cooling system to the cabin was assumed in the study.

2.1. ICE Thermo-Fluid Dynamic Model

The internal combustion engine block is represented by the 1D thermo-fluid dynamic model Gasdyn [39]. The conservation equations of mass, energy, and momentum for an unsteady, ideal, compressible gas flow with friction and heat transfer at the pipe walls, are solved on a one-dimensional domain, representing the ducts, resorting to 0D sub-models and boundary conditions to model pipe junctions, turbochargers, and cylinders. The CG-TVD, or Corberán-Gascón "total variation diminishing" formulation [40], numerical scheme is used for the solution of the conservation equations along the 1D pipe-system; this is an explicit, 2nd order numerical method, with a timestep determined by the Courant–Friedrichs–Lewy (CFL) [41] condition which requires the timestep to be the minimum value of Eq. (1) applied to the whole domain considering the local mesh size Δx, speed of sound υ and gas velocity U.

$$\Delta t = \frac{\Delta x}{\upsilon + |U|} \tag{1}$$

The boundary conditions are instead assumed quasi-steady at each time step, solved by applying a characteristic-based approach. In particular, the compressor and turbine exploit a map-based approach. To decrease the computational effort required by the simulation of long RDE cycles, a 1D numerical solver called FSM (Fast Simulation Method) has been developed and applied, on the basis of the "1D Cell" numerical scheme [34]. This numerical method can provide a good mass conservation also on coarse meshes, allowing to increase the mesh size and the corresponding time step, hence significantly decreasing the simulation time, to reach a CPU/real time ratio around 2.0–2.5. The Fast Simulation Method (FSM) used as solver of the 1D model relies on the strong conservation of mass, typical of finite volume approaches, to significantly increase the mesh size and correspondingly the calculation time step. Recalling Eq. (1), considering the increase of mesh size from 1 cm to 10 cm, the resulting increase of time step size is roughly of one order of magnitude as well. Therefore, the CPU time reduces by 90%. Although, the lumped thermal model is used to model a 3D space, it is a 1D lumped thermal model, hence much faster. Since the overhead computational effort determined by the lumped thermal model is low, in the coupled simulation the overall CPU/real time ratio is determined by the slowest model, which is the 1D fluid dynamic model.

The SI engine combustion process is modelled by a multi-zone approach, to evaluate the thermodynamic properties and chemical composition inside the combustion chamber. The in-cylinder mixture is first divided into two zones, unburnt and burned gas, separated by a flame front, which is assumed to be spherical and infinitesimally thin. The solution of mass and energy equations applied to the burned and unburned zones allows the computation of the pressure and temperature of the two zones. The burnt zone is then further divided into a certain number of zones of equal mass, created during the combustion process. Each zone is spherical, centred on the spark plug and exchanges heat with the cylinder walls, according to the respective surface area. Pressure in the combustion chamber is assumed uniform and the chemical composition is computed in each zone. The solver exploits the Zimont's model to compute the turbulent flame velocity from the laminar velocity, taking account of the turbulence intensity generated in the combustion chamber [34].

The complete 1D model of the 1.0L, 3-cylinder GDI engine has been built, considering a detailed description of the whole intake and exhaust system layout. The maps of the turbocharger have been interpolated and extrapolated, to be suitable for use in the 1D model solver. The complete operating map of the GDI engine has been configured with information concerning for example the air-to-fuel ratio, spark advance timing, variable valve timing actuation, compressor boost pressure target and intercooler efficiency. The corresponding 1D schematic is reported in Fig. 1. The same model has been used to simulate steady state operating points of the engine map and transient RDE operation.

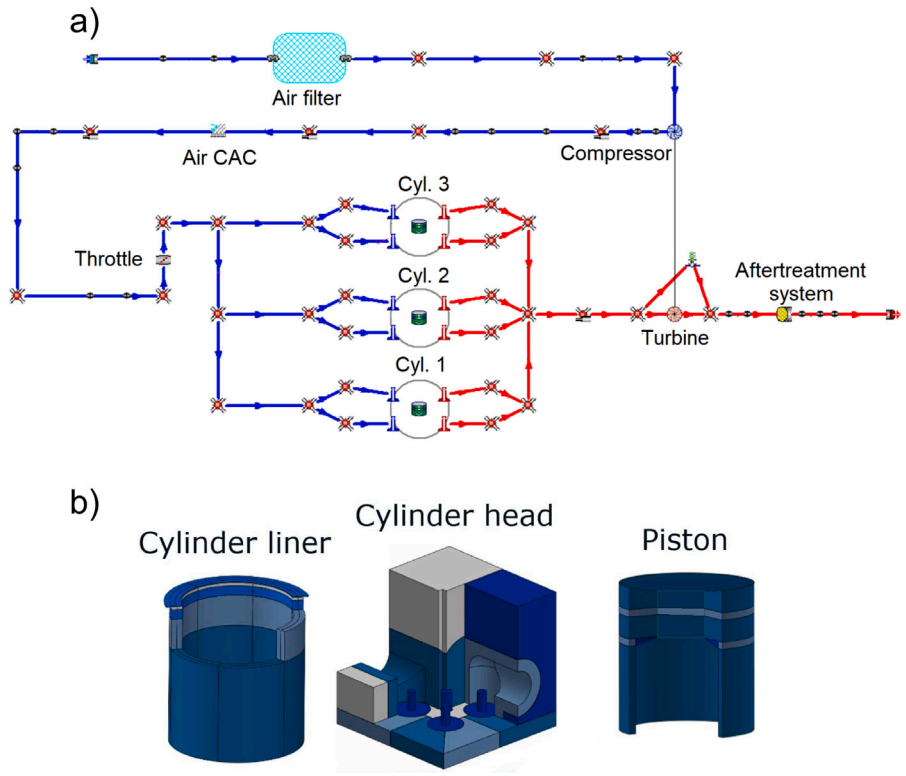

Fig. 1. (a) 1D ICE Thermo-Fluid Dynamic Model, (b) ICE Lumped Thermal Model.

In the 1D schematic the throttle body and the wastegate PID controllers are highlighted, used to control the target torque and boost pressure. The catalytic converter element is also present, to correctly predict the back pressure.

2.2. ICE Lumped Thermal Model

In this section, the ICE thermal model is detailed. This model was the responsible for calculating the temperature distribution in the cylinders of the engine. Regarding its interaction with other submodels, it was interconnected with the ICE gas model and the thermohydraulic model. This model was developed so it could receive as an input the heat rejected from the in-cylinder gas to the material walls (liner, head and piston) which was calculated with the ICE Thermo-Fluid Dynamic Model (Section 2.1).

This model is based on a 1D lumped thermal network approach and is composed by 111 material nodes strategically distributed. The cylinder liner, cylinder-head and piston were divided into 66, 35 and 10 nodes, respectively. Fig. 1 shows the discretization of each part of the engine cylinders. The multiple nodes were considered isothermal and isotropic. They were defined according to the geometry and characteristics of the engine given by the manufacturer. Each node had its volume, density, thermal capacity and conductivity. Additional to the material nodes, 6 fluid nodes were included in order to account for the heat rejected to the coolant and oil. Both inlet and outlet nodes of coolant thorough the liner (2 nodes) and cylinder-head (2 nodes) were implemented. Similarly, inlet and outlet nodes of oil were included. It is important to note that inlet nodes served as boundary conditions and were imposed by the values given by the thermohydraulic model (Section 2.3). In Fig. 3, the integration of the ICE Lumped Thermal Model with the other submodels of the ICE is presented (where the main interaction among these models are shown).

The heat transfer mechanisms considered in the ICE thermal model were conduction (among the solid material nodes) and convection (between the material and the fluid) as it can be observed in Eqs. (2) and (3). These equations were obtained from performing the energy balance for each node. In order to increase the stability of the solver, an implicit numerical method for solving the equations was implemented.

$$m_i\, c\left(\frac{T^i_{t+\Delta t}-T^i_t}{\Delta t}\right)=\sum_j \frac{k_{ij}\,A_{ij}}{d_{ij}}\left(T^j_{t+\Delta t}-T^i_{t+\Delta t}\right)+\sum_k \dot{Q}_{g\to i}+\sum_l h_{li}\,A_{li}\left(\frac{T^{l,ou}_{t+\Delta t}+T^{l,in}_{t+\Delta t}}{2}-T^i_{t+\Delta t}\right) \tag{2}$$

where m_i, c, k_{ij}, A_{ij} stand for node mass, heat capacity, thermal conductivity and contact area between solid nodes i and j, respectively. Additionally, $T^i_{t+\Delta t}$ and T^i_t are the current node temperature and the node temperature for the previous calculation step. $\dot{Q}_{g\to i}$ is the heat generated or rejected from the gas to the wall nodes. d_{ij} is the distance between solid nodes while h_{li} is the convection heat transfer coefficient between solid (i and j) and liquid (l) nodes.

$$\frac{m_l\,c_p}{\Delta t}\left(\frac{T^{l,ou}_{t+\Delta t}+T^{l,in}_{t+\Delta t}}{2}-\frac{T^{l,ou}_{t}+T^{l,in}_{t}}{2}\right)+\dot{m}_l\,c_p\left(T^{l,ou}_{t+\Delta t}-T^{l,in}_{t+\Delta t}\right)=\sum_l h_{jl}\,A_{jl}\left(T^i_{t+\Delta t}-\frac{T^{l,ou}_{t+\Delta t}+T^{l,in}_{t+\Delta t}}{2}\right) \tag{3}$$

where m_l, c_p and $\dot{m}_l$ represent the mass, heat capacity and flow mass of liquid nodes, respectively.

Furthermore, the equations were rearranged in a matrix array aiming to reduce the simulation time as it is seen in Eq. (4).

$$[T_{t+\Delta t}]_{nx1}=\left([K]_{nxn}-[C]_{nxn}\right)^{-1}\left([T^{bc}]_{nx1}-[C]_{nxn}[T_t]_{nx1}\right) \tag{4}$$

where n is the total number of nodes. $[T_{t+\Delta t}]_{nx1}$ is the array of nodes temperature for the next calculation step while $[T_t]_{nx1}$ is the vector of temperatures for the current time. $[K]_{nxn}$ and $[C]_{nxn}$ represent the thermal conductances and capacitances, respectively. $[T^{bc}]_{nx1}$ is the

boundary condition array and consists of temperature or heat values of the nodes considered as boundary condition (i.e. coolant inlet temperature, oil inlet temperature or solid nodes in contact with the in-cylinder gas in which heat is generated). It is important to note that the boundary conditions are directly dependant on the integration of the submodel. In other words, the defined inputs of the submodel determined the number of nodes taken as a boundary condition.

2.3. ICE Thermohydraulic model

The 0D/1D thermohydraulic model was responsible for calculating the temperatures, flows and pressures in the circuits of the different thermal management systems present in the propulsive system of an PHEV. The same source code was used for developing the different hydraulic circuits of the hybrid propulsive system. These include the TMS of the ICE, battery and EDS. Additionally, a thermohydraulic model was also developed for the lubricant circuit of the engine.

The thermo-hydraulic model is based on Eqs. (5)–(7). Once the geometry and the layout of the circuits are interpreted by the model, its solver calculates the pressure and flows by applying the continuity and energy conservation laws for each closed loop of the circuit. Afterwards, in order to calculate the temperature distribution, the circuits is divided into several fluid volumes and the energy balance is performed according to Eq. (7) for each volume.

$$\sum \dot{V} = 0 \tag{5}$$

$$\sum R_2 \dot{V}^2 + \sum R_1 \dot{V} + \sum R_0 = 0 \tag{6}$$

where R_2, R_1 and R_0 represent the quadratic, linear and independent coefficients of the hydraulic resistance respectively. Additionally, $\dot{V}$ is the volumetric flow mass.

$$\frac{m_{fv}\, c_p}{\Delta t}\left(T_{t+\Delta t} - T_t\right) = K_{fa}\left(T_{amb} - T_{t+\Delta t}\right) + \dot{Q} \tag{7}$$

where T_t is the current temperature of fluid volume, $T_{t+\Delta t}$ is the temperature of the fluid volume in the next time step, m_{fv} corresponds with the mass of the fluid volume and c_p is the fluid heat capacity. K_{fa} stands for the equivalent heat conductance between fluid and ambient. This parameter accounts for the heat conductivity and convection processes. Finally, the T_{amb} is the ambient temperature while $\dot{Q}$ represents the heat exchanged with other submodels (i.e. heat rejected from the ICE to coolant).

The coolant and oil circuits of the engine were formed by several different elements. Fig. 2 shows both the layout of the engine hydraulic circuits. For the coolant circuit, the geometry (i.e. length and diameter) was experimentally measured for the accessible pipes while for the oil, a simplification of the circuit was taken and only the main paths and components were implemented in the model according to the data provided from the manufacturer.

It is important to highlight that the coolant circuit used in the test bench was not exactly the same as the one implemented in the vehicle. For instance, the aerotherm was not installed in the test bench and was replaced by a pipe. The radiator was replaced by a controlled water/water heat exchanger of shell a and tubes in order to improve the control over coolant temperature. The lengths of some paths were slightly different because of the addition of the instrumentation (i.e. flow meters) in the circuit.

The main pump of the coolant circuit was characterized by its volume, speed ratio between pump and engine, head pressure and efficiency curves. The speed of this turbopump depended on the engine regime. According to the experimental data, the coefficients of the curve were calibrated. This component provides the necessary pressure and flow for the correct operation of the system. Additionally, the pipes were defined by their diameter, length and friction coefficient. The thermostat was modelled as a valve which creates a localized hydraulic resistance depending on the thermostat opening lift. Likewise, this opening lift is function of the coolant temperature as it was detailed in the [36]. The implementation of the heat exchangers was performed for the engine cylinders, the turbocharger, radiator and the oil cooler. They were defined by their volume, type (i.e. shell and tubes) and hydraulic resistance coefficients. The heat flux calculated by the ICE Lumped Thermal Model is transferred to the coolant by means of this heat exchanger. For the case of the heat rejected by the turbocharger, the experimental luck up table (i.e. calculated using the flow and temperature difference) is used as input in the simulations. The oil cooler is a heat exchanger responsible of the thermal interaction between the coolant and the oil circuit. It also produces a pressure drop depending on the flow rate. The heat exchanged between both fluids (oil and coolant) is calculated according to the NTU (Number Transferred Units) method. For the radiator, a heat exchanger with controlled outlet temperature was implemented as it was performed in the test bench.

According to Fig. 2, five well-differentiated coolant branches are observed after the engine outlet. Through the thermostat to the radiator, across the bypass to the main pump, to the oil cooler, to the turbocharger or through the pipe replacing the aerotherm. These two last paths merge into the aerotherm branch as it can be seen in Fig. 2. For the sake of clarity, two thermostats are showed in Fig. 2. The one named thermostat represents the element in the path to the radiator while the bypass one, corresponds with the element situated in the coolant path when thermostat is closed.

The coolant flow in each branch is described as follows:

- Radiator and by-pass branch: This branch has two paths depending on the coolant temperature. The thermostat opening determines the amount of flow that circulates in each path according to the temperature of the coolant and ECU (Electronic Control Unit) signal. When the engine is cold, i.e. thermostat closed, the fluid will flow through the internal by-pass of the engine, a path that will take the fluid directly to the engine inlet. As the engine temperature increases and therefore thermostat starts to open, part of the flow will be derived to the radiator branch, where heat will be rejected to the environment. Finally, when thermostat is completely opened, coolant will not flow through the by-pass branch. Additionally, the radiator branch forms an additional loop with the expansion tank.
- Oil cooler branch: This branch contains the oil cooler, which is in charge of cooling the oil. The coolant is extracted from engine internal circuit and return to water pump inlet. This is the element connecting both coolant and oil circuit
- Aerotherm branch: The remaining branch of the circuit is the one that contains both the replaced aerotherm and the turbocharger. In this branch, the merging between the flow coming from the turbocharger and the one coming from the aerotherm (replaced by a pipe in the test bench as previously mentioned).

Similarly, the oil circuit is composed by the cylinder heat exchangers, turbocharger heat exchanger, and the oil cooler. Additionally, a positive displacement pump was implemented as it can bee seen in Fig. 2. The characterization process was similar to the one taken for the coolant circuit. The heat rejected by the cylinders (mainly by the piston) was calculated by the ICE Lumped Thermal Model.

The engine speed is a boundary condition of the ICE Thermohydraulic Model which will determine the speed of both coolant and oil pumps. Additionally, the ambient temperature is needed as an input so the heat transfer with the ambient is taken into account. Finally, the heat rejected to coolant and oil are also a fundamental input to the model. Fig. 3 presents the overall integration of the ICE models.

2.4. Battery

To estimate the heat rejected by the battery pack, a first order Equivalent Circuit Electric Model (ECEM) for a battery cell was developed using reliable data from bibliography and available experimental

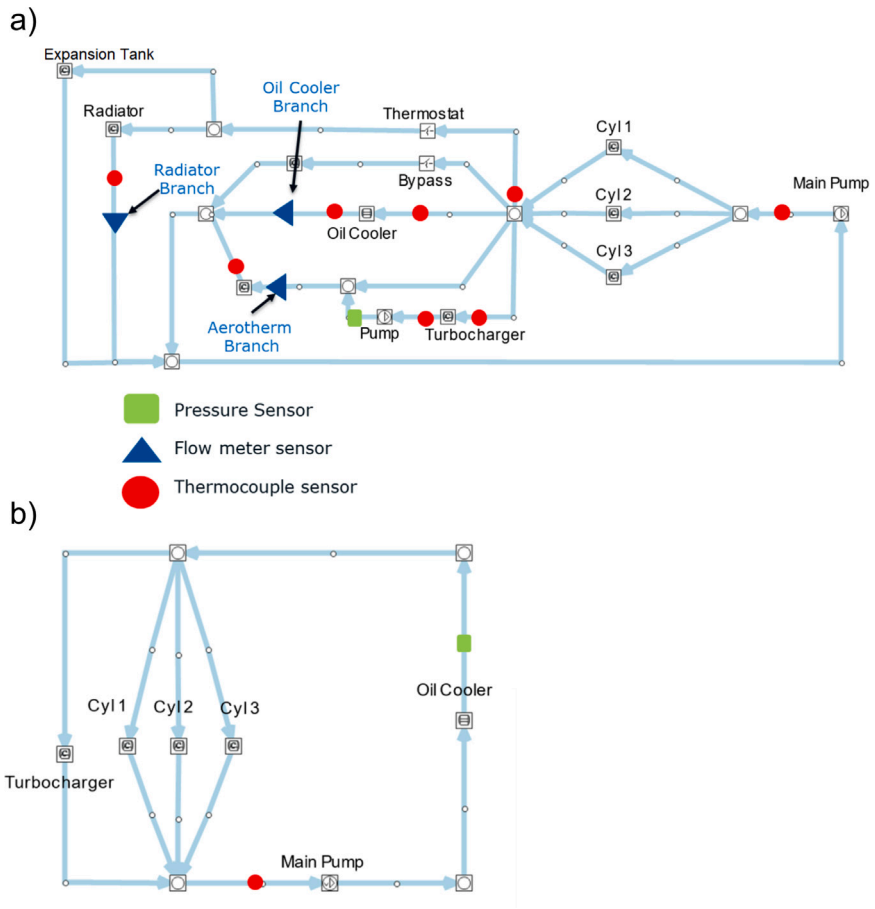

Fig. 2. (a) ICE coolant circuit layout, (b) ICE oil circuit layout.

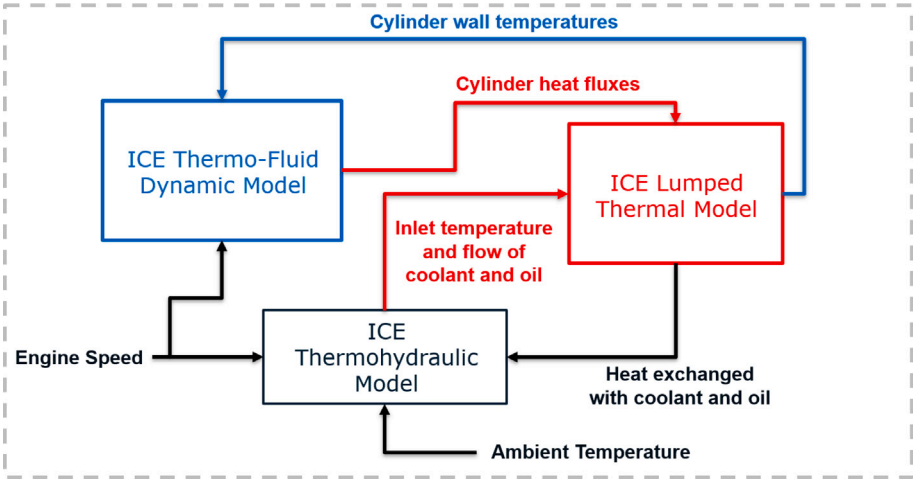

Fig. 3. Integration of ICE Lumped Thermal Model, ICE Thermo-Fluid Dynamic Model and ICE Thermohydraulic Model.

measurements. Fig. 4 presents the scheme of the solved electric circuit. The parameters of the circuit were obtained from the experimental measurements performed by Pirooz et al. [42]. The detailed methodology for the optimization of the model is fully described in [38]. The heat generated in the cells is calculated according to Eq. (8). The power supplied and required by the battery is determined by the strategy established by the control model of the vehicle during the cycle. This strategy aimed to increase fuel savings and battery charge sustain. The electric power exchanged from the battery pack is divided by the total number of cells and set as an input to the ECEM which solves the equivalent electric circuit and calculates the heat power generated in one cell. Afterwards, this heat power is multiplied by the total number of cells to calculate the total heat power rejected by the battery pack to the cooling system.

$$\dot{Q}_{cell} = I_{cell} * (E_o - V_{cell}) \tag{8}$$

where the $\dot{Q}_{cell}$ is the heat generated in the cells of the battery, I_{cell} is the cell electric current, E_o is the open circuit voltage and V_{cell} is the cell voltage.

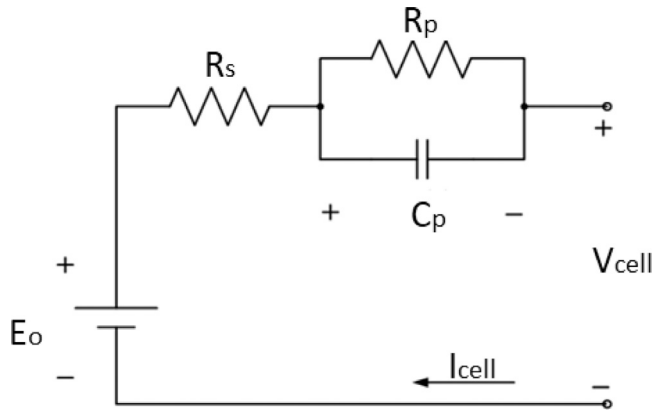

Fig. 4. First order ECEM of the battery cells.

Table 1
Features of the battery cells.

Parameter	Value
Chemistry	LTO
Shape	Prismatic
Nominal voltage (V)	2.3
Nominal capacity (Ah)	23
Weight (kg)	0.55
Volume (L)	0.26
Dimensions L ∗ W ∗ H (mm)	115 ∗ 22 ∗ 103

The battery pack was constructed by 144 prismatic 23 Ah LTO battery cells. The cell characteristics are summarized in Table 1.

The battery pack was divided into 12 modules of 12 cells each one. The thermal management system (TMS) defined for cooling the cells was based on an indirect cooling through the cell base using a cooling plate. This TMS was divided into 6 paths of coolant running under the battery modules (see Fig. 5). Additionally, computational fluid dynamic (CFD) results obtained from previous work were used to calculate the pressure drop across the battery thermal management system [43]. Fig. 5 shows the velocities and the coolant paths through the TMS. First, calculations at different coolant flows (from 0.5 kg/s to 2.5 kg/s) were performed. Then, the obtained pressure drop for each coolant flow was used to determine the hydraulic resistance coefficient according to Eq. (9).

$$\Delta P = K\dot{m}^2 \tag{9}$$

where ΔP is the total pressure drop, K is the hydraulic resistance coefficient and $\dot{m}$ is the mass flow rate.

Fig. 7 (left) shows the scheme of the battery thermal management system (BTMS). This BTMS was constructed using a main heat exchanger (named Battery in Fig. 7) which will be responsible to dissipate the heat rejected by the battery pack to the coolant. The selected coolant was based on a mix of Glycol (50%) and water. This heat power is calculated by using the ECEM approach as it was previously stated. Additionally, the BTMS also includes a pump, a cooler/heater, a thermostat which starts opening when the coolant temperature at the outlet of the battery reaches 30 °C and different pipes to connect the elements. The coolant flow propelled by the pump was set constant and calculated considering the maximum heat rejected by the battery pack in the complete cycle and a maximum temperature drop across the BTMS of 2 °C. According to the literature, one of the objective of the BTMS is to decrease the temperature gradient through the battery pack. Hence, decreasing this temperature drop will directly impact the temperature gradients among the cells.

2.5. Electric drive system

The electric machine of the EDS had a maximum torque and power of 200 N m and 50 kW, respectively. For calculating the heat rejected by the EDS (acting as a Motor or Generator), two efficiency maps were implemented, one for each of the two mentioned actuations. The maps are shown in Fig. 6. Given the fact that the efficiency shows a small dependence with the voltage, the nominal voltage of the battery pack (V) was considered as input for the efficiency maps ((N, V)). Similarly to the battery case, the required mechanical power and the generated electrical power by the EDS are determined by the control of the vehicle model. With the EDS power (P_{req}) and its speed (N), the heat rejected ($\dot{Q}_{EDS}$) to the coolant is calculated by using the maps of Fig. 6, according to Eq. (10).

$$\dot{Q}_{EDS} = P_{req}\frac{\eta(1-\eta(N,V))}{\eta(N,V)} \tag{10}$$

The electric drive thermal management system (EDTMS) is very similar to the BTMS. The layout is presented in the right-hand side of Fig. 7. In this system a pump that supply a constant coolant flow equal to the 17% of the ICE maximum coolant flow is considered. This performance was decided following the same criterion as for the battery cooling system, taking the maximum heat rejected during the cycle and setting the temperature drop to 2 °C. This element was implemented in the thermohydraulic model by means of a heat exchanger. Finally, this TMS also includes a thermostat that starts opening when the temperature of the coolant at the outlet of the electric drive reaches 60 °C and is completely open at 70 °C.

2.6. Integrated thermal management system

The powertrain elements of a hybrid vehicle operate at three different levels of temperature. The ICE has the highest working temperatures (≈80–90 °C), the EDS is the system with the medium temperatures (≈50–60 °C) while the battery pack requires the lowest operation temperature (≈15–35 °C). This situation, forces to consider a dedicated thermal management system (TMS) for each element to maintain the temperature in the required operable ranges. Two concepts of thermal management systems were considered.

The features of the TMS that have been considered in this analysis for each element are the following:

- ICE: To reduce warm up time (time the coolant needs to reach 85 °C) and to avoid temperature drop at engine stops.
- EDS: Maintaining the coolant temperature below 60 °C.
- Battery: Keeping the coolant temperature between 20 °C and 35 °C the maximum time.

The “independent” TMS system is based on designing a particular coolant circuit for each element of the powertrain of the hybrid vehicle. This case was taken as the baseline from which different layouts were explored. Although it is the less complex one, it does not allow the interaction of heat flows between the different systems.

The “integrated” two new heat exchangers (HX) were implemented in order to study the interaction among the available thermal flows and explore the synergies between the three-level temperature systems of the hybrid powertrain. These elements allow the interaction between the high (ICE) and medium (EDS) temperature circuits and between the medium (EDS) and low (Battery) temperature circuit of the TMS. Fig. 8 shows the layout of the integrated thermal management system. The low temperature HX connects the coolant circuit of the battery with the coolant circuit of the EDS while the high temperature HX connects the thermal flows between ICE coolant circuit and EDS coolant circuit. One of the main criteria for designing such thermal management systems was the use of the minimum elements as possible and trying to eliminate redundant components. For instance, the cooler of the independent TMS was eliminated since the preliminary results showed that keeping

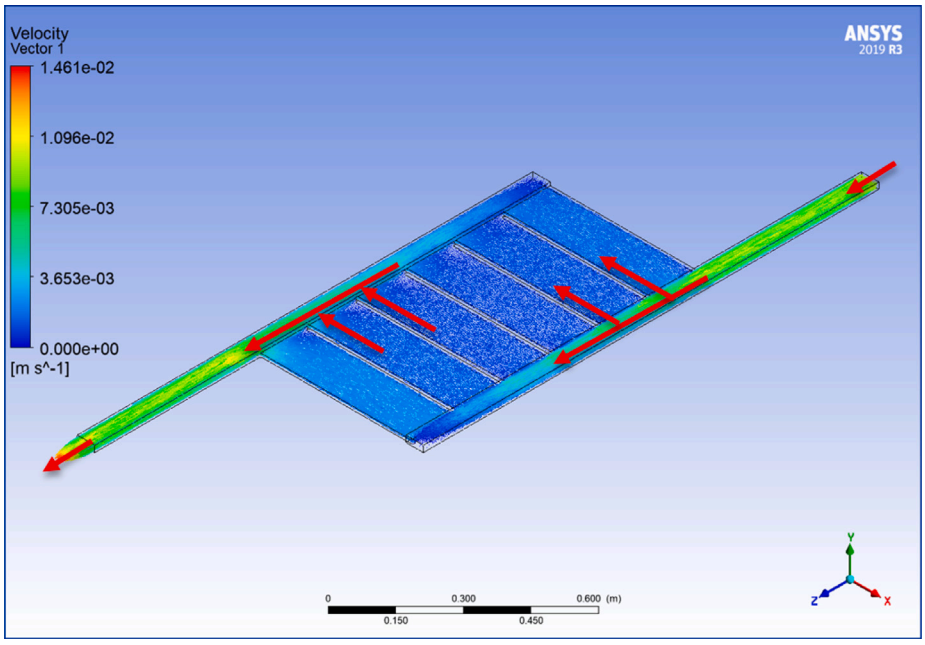

Fig. 5. Coolant path of Battery TMS (CFD).

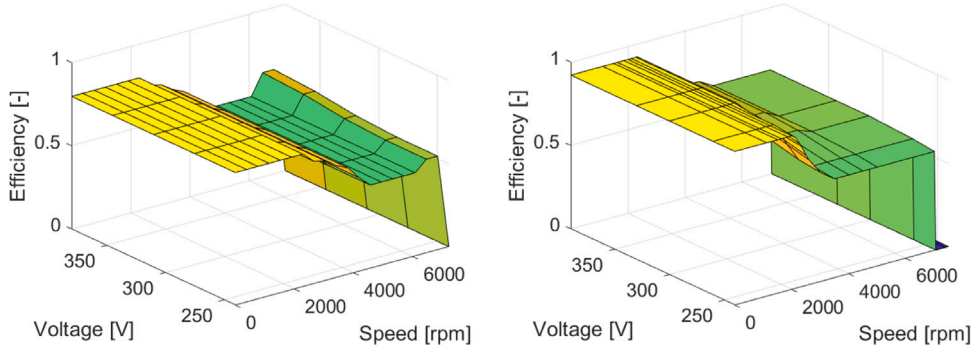

Fig. 6. EDS efficiency maps, working as generator (left) and motor (right).

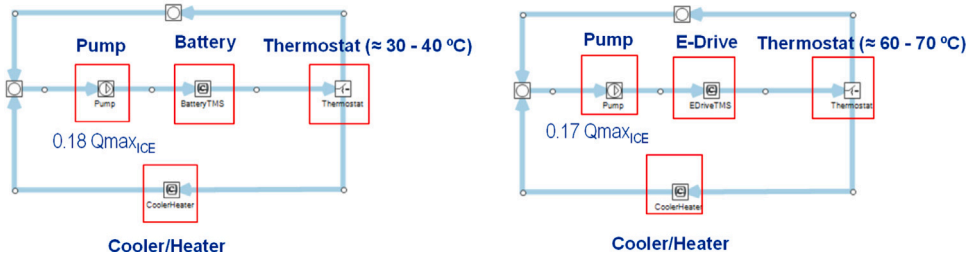

Fig. 7. Battery TMS (left) and electric drive system TMS (right).

the battery cooler was suitable. Additionally, an actuated valve was implemented in the EDTMS to avoid cooling the ICE when it could be detrimental for fuel economy and emissions. For this purpose, this valve is completely closed when the ICE coolant temperature reaches 60 °C disconnecting the low temperature fluid (EDS coolant) side of the high temperature HX.

Overall, the number of elements for each layout is summarized in Table 2. By adding two additional components it is possible to get benefits from the thermal flow interaction depending on the requirements of the different subsystem.

Table 2
Number of components of the TMS layouts.

Components	Independent TMS	Integrated TMS
Pumps	3	3
Cooler/Heater	3	2
Thermostat	3	3
Heat exchanger	0	2
Actuated valve	0	1
Total	9	11

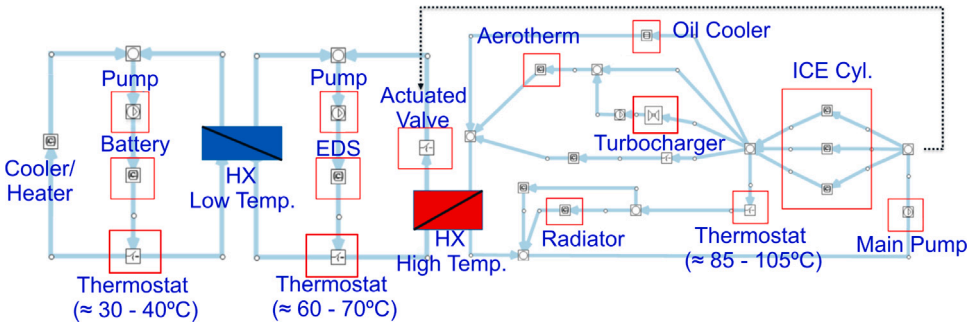

Fig. 8. Integrated thermal management system.

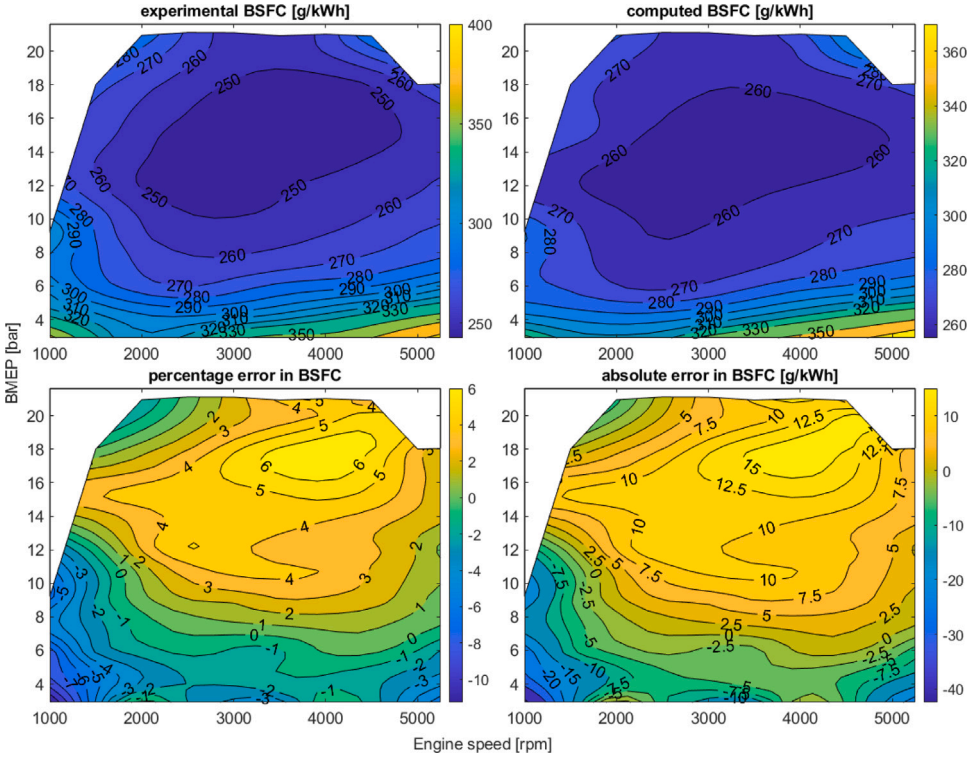

Fig. 9. Experimental validation of ICE fuel consumption.

3. Experimental testing

In this section a description of the experimental campaign performed with the ICE is presented. This engine is a 3-cylinders 1L Gasoline engine. The measurements were performed in a highly instrumented test bench. The test bench was equipped with state-of-art components that allow the operation of the engine in RDE transient conditions. Additionally, the experimental campaign performed for this work considered several steady state running conditions within the engine performance map. The tested conditions have been the following:

- Ten points ranging from 1000 rpm to 5250 rpm at full load: they were used, first to validate engine simulations and secondly to adjust hydraulic parameters.
- Ten points going from 1000 rpm to 5250 rpm in motoring conditions. They have been used to obtain the main uncertainties of the engine: compression ratio, heat transfer coefficients, thermodynamic delay and deformations coefficient. These are parameters for the combustion analysis tool (CALMEC) in which the main experimental input is the in-cylinder pressure signal. The first law of thermodynamics is applied between IVC (intake valve closing) and EVO (exhaust valve opening) to calculate the rate of heat release as the main result [44,45]. Among the results, the heat rejected to the coolant and oil is also calculated, which served to calibrate the heat rejected to the hydraulic circuits.
- Sixty-three points from low load (3 BMEP) to high load (around 22 BMEP) covering a wide range of the engine map.

Table 3
Engine specifications used for validation of the ICE models.

Parameter	Value
Displacement	999 cm^3
Diameter	81.3 mm
Stroke	72.2 mm
Number of cylinders	3 in line
Number of valves	4 per cylinder
Max torque @ speed	182.3 N m @ 2250 rpm
Max power @ speed	83.0 kW @ 5250 rpm

The engine features are summarized in Table 3.

The test bench was equipped with different measurement tools that were thoroughly calibrated before the measurement campaign. Several

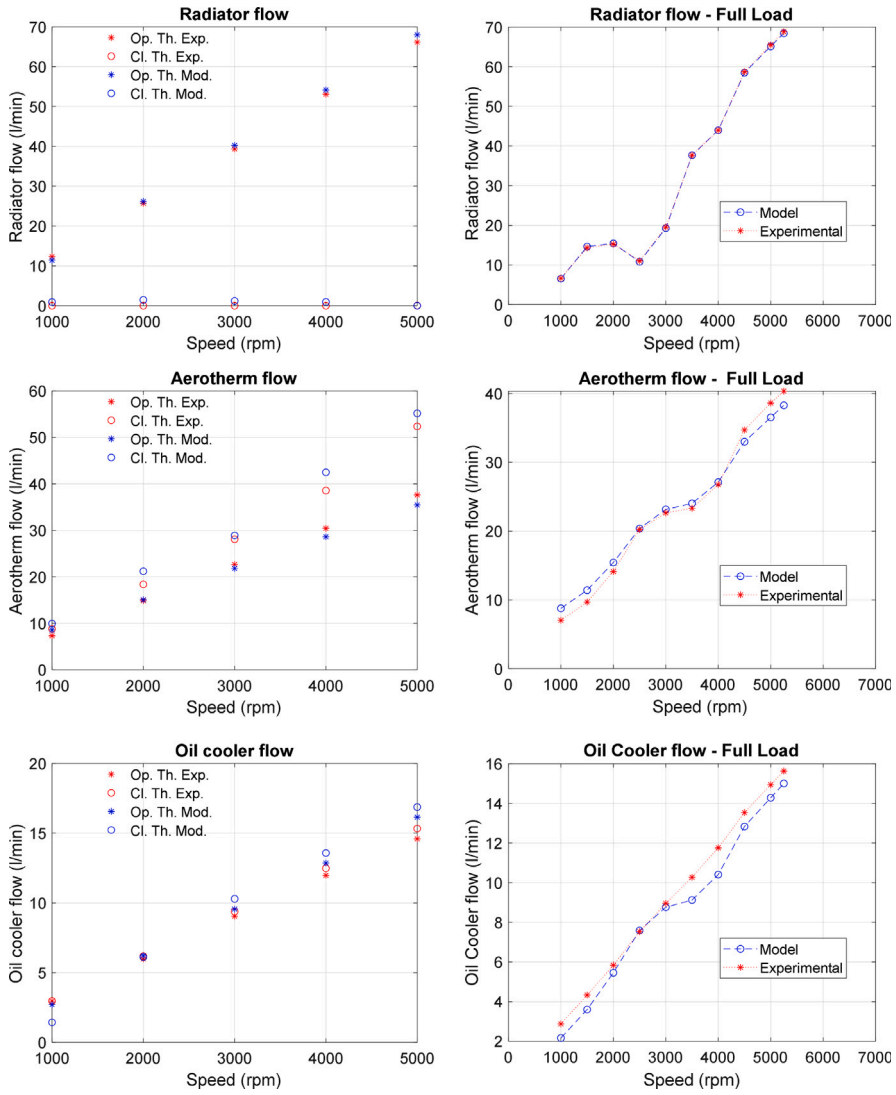

Fig. 10. Validation of the additional coolant flow measurements with thermostat open (Op) and closed (Cl) for radiator (a), aerotherm (b) and oil cooler (c). Flows validation at full load conditions for radiator (d), aerotherm (e) and oil cooler (f).

Table 4
Laboratory instrumentation.

Variable	Instrument	Range	Accuracy
Engine speed	Dynamometer	0–7500 rpm	±1 rpm
Torque	Dynamometer	0–400 N m	±0.5%
Fluid temperature	k-type thermocouple	70–1520 K	±2 K
Air mass flow	Flowmeter	0–1700 kg/h	±2%
In-cylinder pressure	AVL GH13P	0–200 bar	±0.3%
Coolant flow	OPTIFLUX 4000	4.5–90 lpm	±0.5%
Oil pressure	Piezoresistive transducer	0–10 bar	±25 mbar
Emissions	Horiba MEXA @ AVL Smoke meter		

temperature, mass flow and pressure sensors were installed in the gas circuit and the hydraulic circuits of the engine. All of them calibrated and connected to a data acquisition system. Table 4 summarizes the main instrumentation equipment.

Temperatures and pressures were measured at the compressor inlet and outlet, at the intake manifold, at the turbine inlet and outlet, at the exhaust manifold and at the inlet and outlet of the exhaust gas after-treatment system. The in-cylinder pressure was measured in one cylinder.

4. Model validation

In this section, the validation of the ICE submodels is presented. For the case of the battery model, it is critical the correct calibration of the heat rejected to coolant circuit. This heat mainly depends on the correct optimization of the electric parameters of the Equivalent Circuit Electric Model as it was presented in the previous section. The parameters used in this work were obtained using experimental measurements that were performed out of the scope of the present work [42]. For the electric drive system, in order to calculate the heat generated, the experimental efficiency maps provided by the manufacturer were used. Hence, only the experimental validation of the ICE submodels is detailed.

4.1. Steady state

In this section the validation of ICE submodels in steady state conditions are presented. For the thermohydraulic model, the validation process was performed in two steps. Firstly, the coolant flows were compared with the measurements followed by a fitting process in which the hydraulic resistances were adjusted. Secondly, the predicted temperatures were compared with the measurements performed in the test bench. In this case, both the thermo-hydraulic model and the

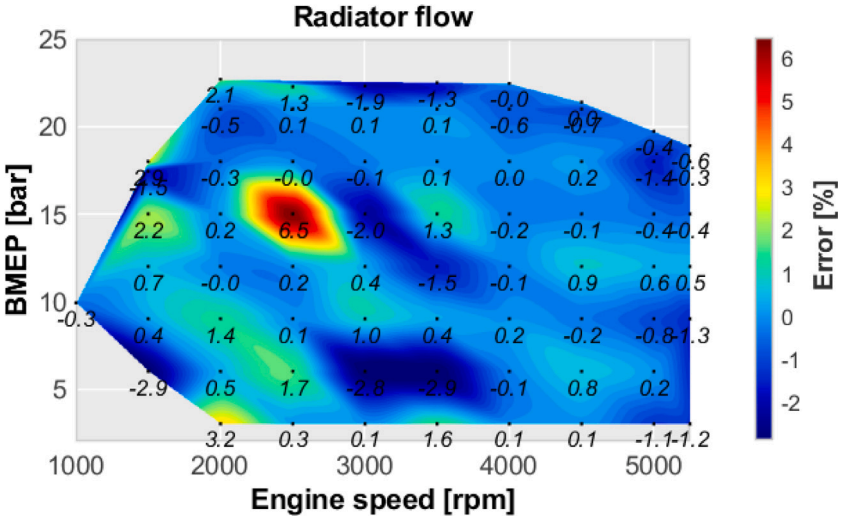

Fig. 11. Radiator branch flow validation.

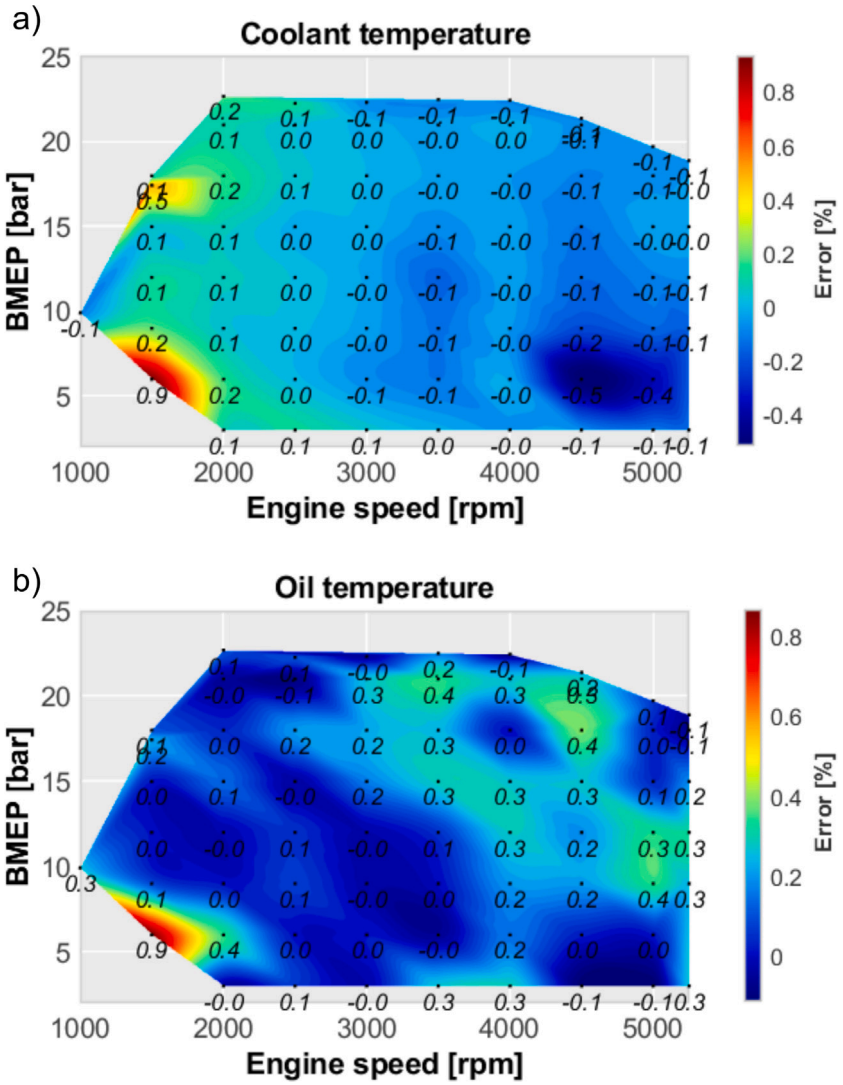

Fig. 12. Engine inlet coolant temperature (a) and oil (b) validation.

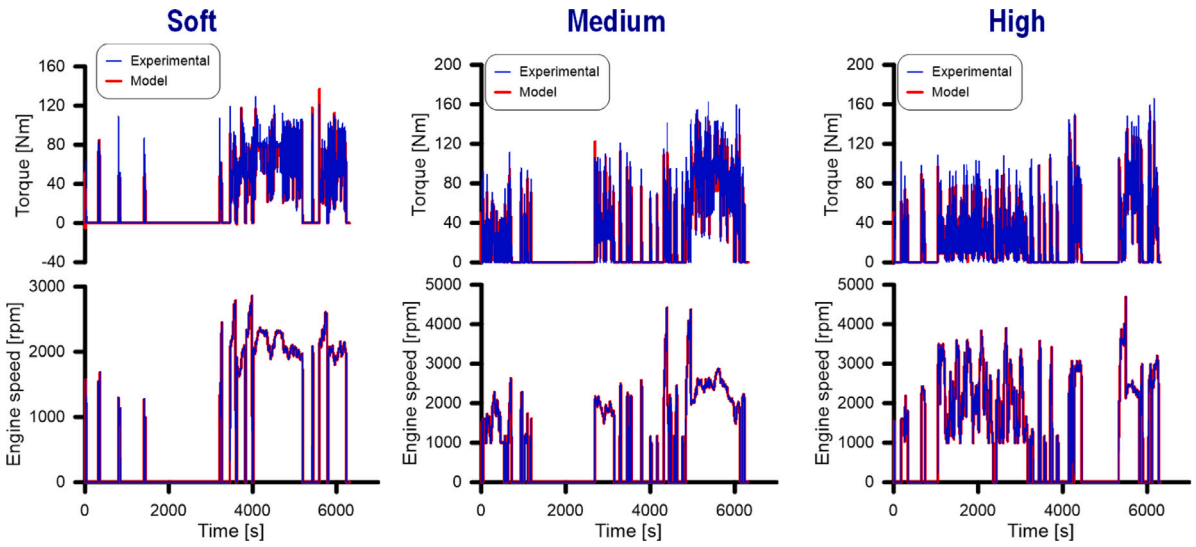

Fig. 13. Validation results for engine performance for RDE cycles.

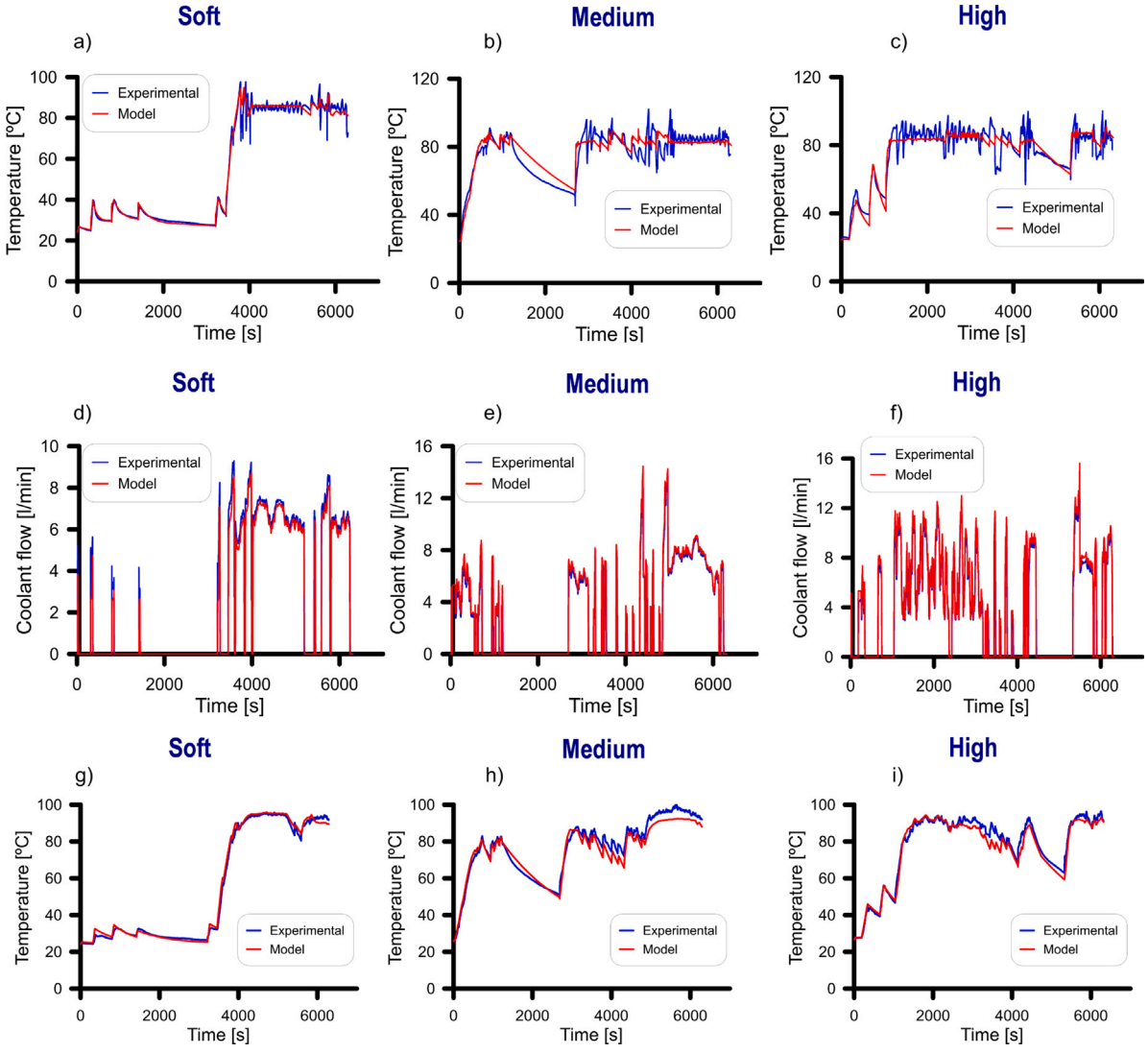

Fig. 14. Validation of coolant engine inlet temperature (a,b and c), oil cooler coolant flow (d,e and f) and oil temperature (g,h and i) in RDE cycles.

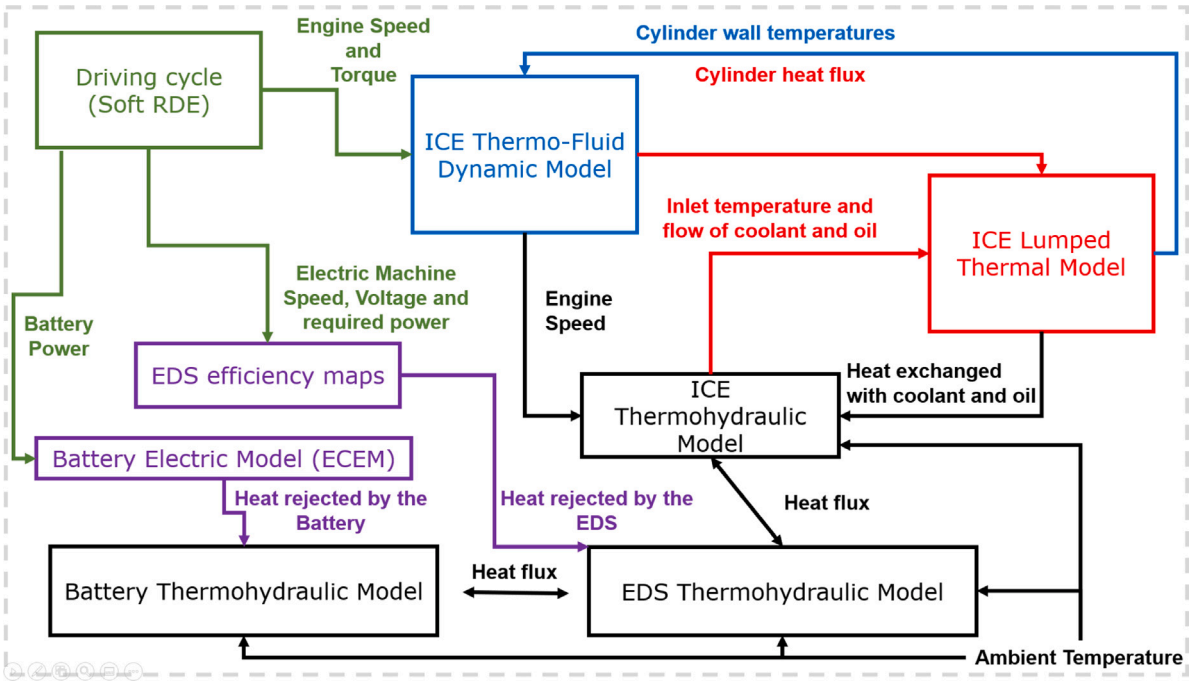

Fig. 15. Thermal integrated co-simulation of an hybrid propulsive system.

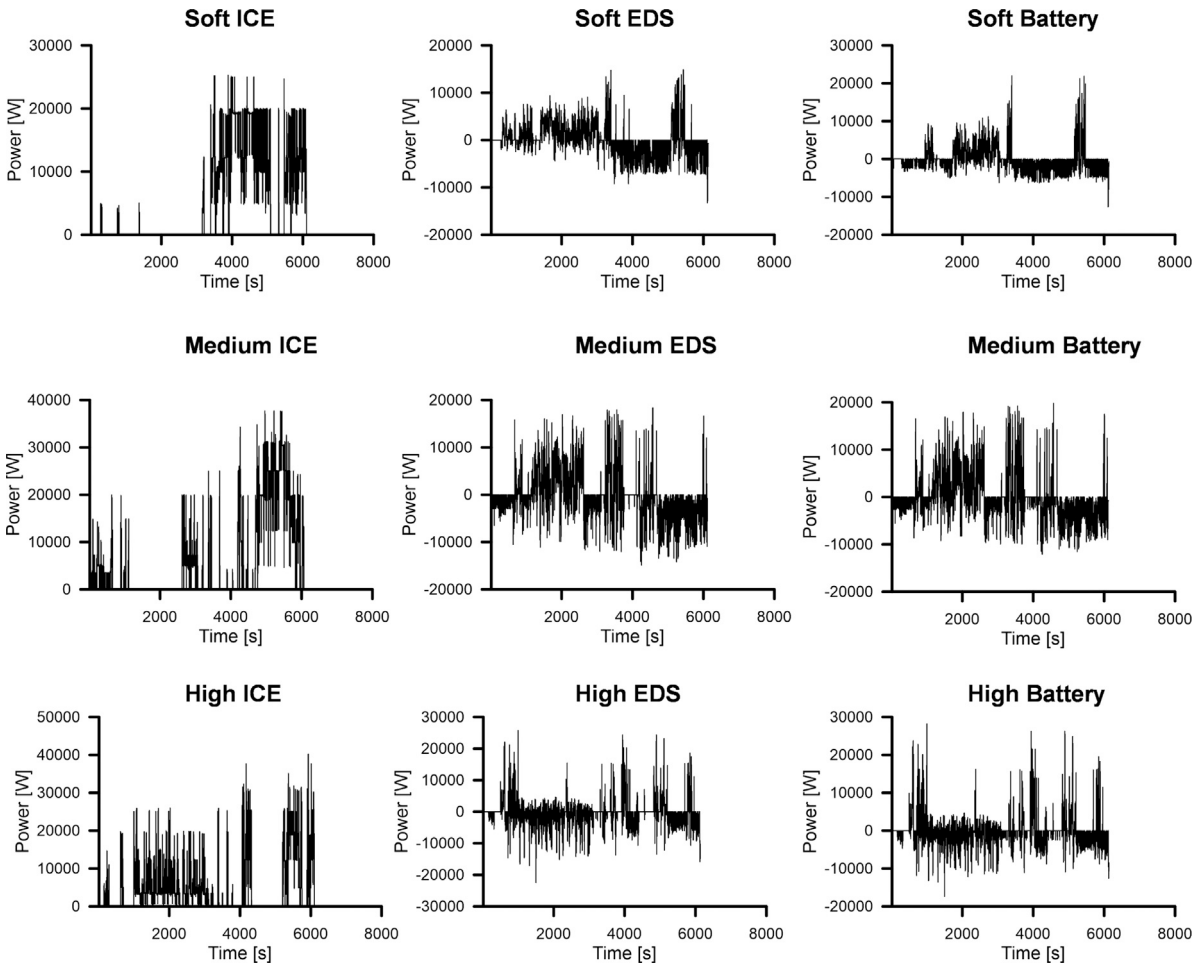

Fig. 16. Power demanded from ICE, battery and EDS subsystems during the RDE cycles.

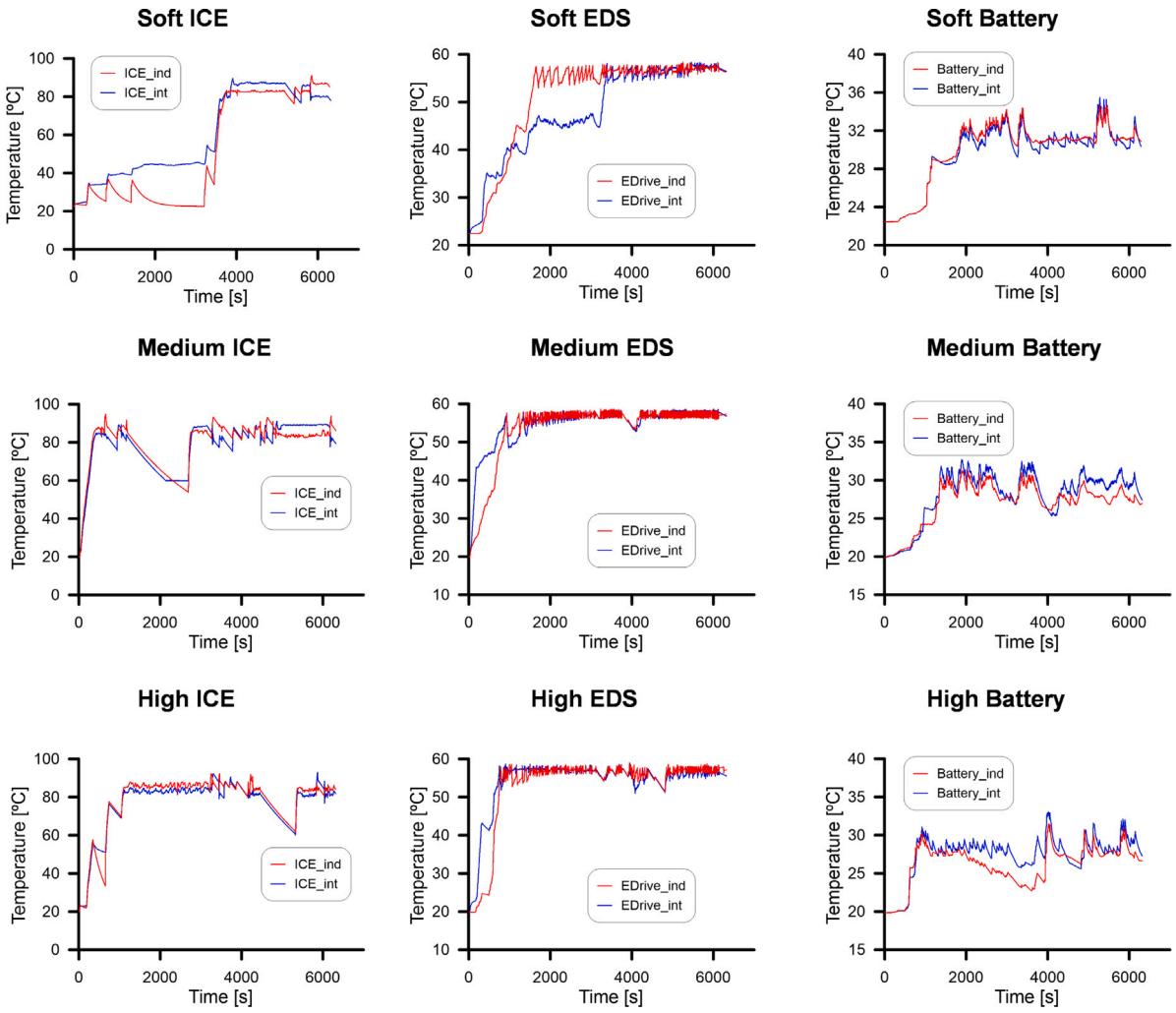

Fig. 17. ICE, battery and EDS coolant temperature evolution for warm conditions in RDE cycles for individual TMS and integrated TMS where, in the legend, the *ind* indicates independent and *int* refers to integrated.

engine model are needed to accurately predict the heat rejected by different elements to the thermo-hydraulic model.

4.2. ICE fuel consumption

The Gasdyn 1D model has been validated on a steady state map of measured operating conditions. A general satisfactory agreement has been achieved. The measured brake mean effective pressure was well matched in all operating points, with a PID controller acting on the throttle opening, whereas the target boost pressure has always been reached by acting on the wastegate opening with a PID controller. Fig. 9 shows the contour plots of the measured and computed brake specific fuel consumption for a direct comparison. The corresponding relative and absolute errors on the whole steady state engine map are presented as well. Overall, the agreement is good, with few regions characterized by a maximum error around 5%, showing a good quantitative and qualitative prediction level in general. This result is very important, allowing the use of the 1D engine model across non-mapped operating conditions during the simulation of RDE driving cycles, where the focus is on the evaluation of cumulative fuel consumption during transient operation.

4.2.1. Hydraulic flows

In order to validate the coolant flows, additional measurements were required for modelling the behaviour of the thermostat.

- First, measurements at different engine speeds with the thermostat closed were used to adjust the flows through the oil cooler and aerotherm branches. Fig. 10 shows the predicted versus measured volumetric flow rate of the coolant across the radiator, aerotherm and oil cooler branches for both open and closed thermostat positions.
- Afterwards, the measurements with thermostat completely open and closed were used to calibrate the coolant flow in radiator's branch and to determine the hydraulic resistance of the thermostat when thermostat is completely open.
- Finally, the full load operating points were used for calibrating partial openings of the thermostat. Fig. 10 shows the results obtained for full load when only the opening degree was modified. The model seems to slightly over-predict the aerotherm flow at low speeds and slightly underestimate it for high speeds. For the case of the oil cooler, the model seems to slightly underestimate the flows for speeds higher than 3500 rpm.

The process followed for adjusting the thermostat allowed to capture both the maximum and the minimum values of the radiator flow (maximum and minimum opening degree).

The parameters modified for the fitting process were the friction of the pipes, the hydraulic resistance of the heat exchangers (radiator, oil cooler, cylinders, turbocharger) and the hydraulic resistance of the thermostat. Note that for the case of the thermostat, its hydraulic resistance depends on its opening degree, and this changes with the

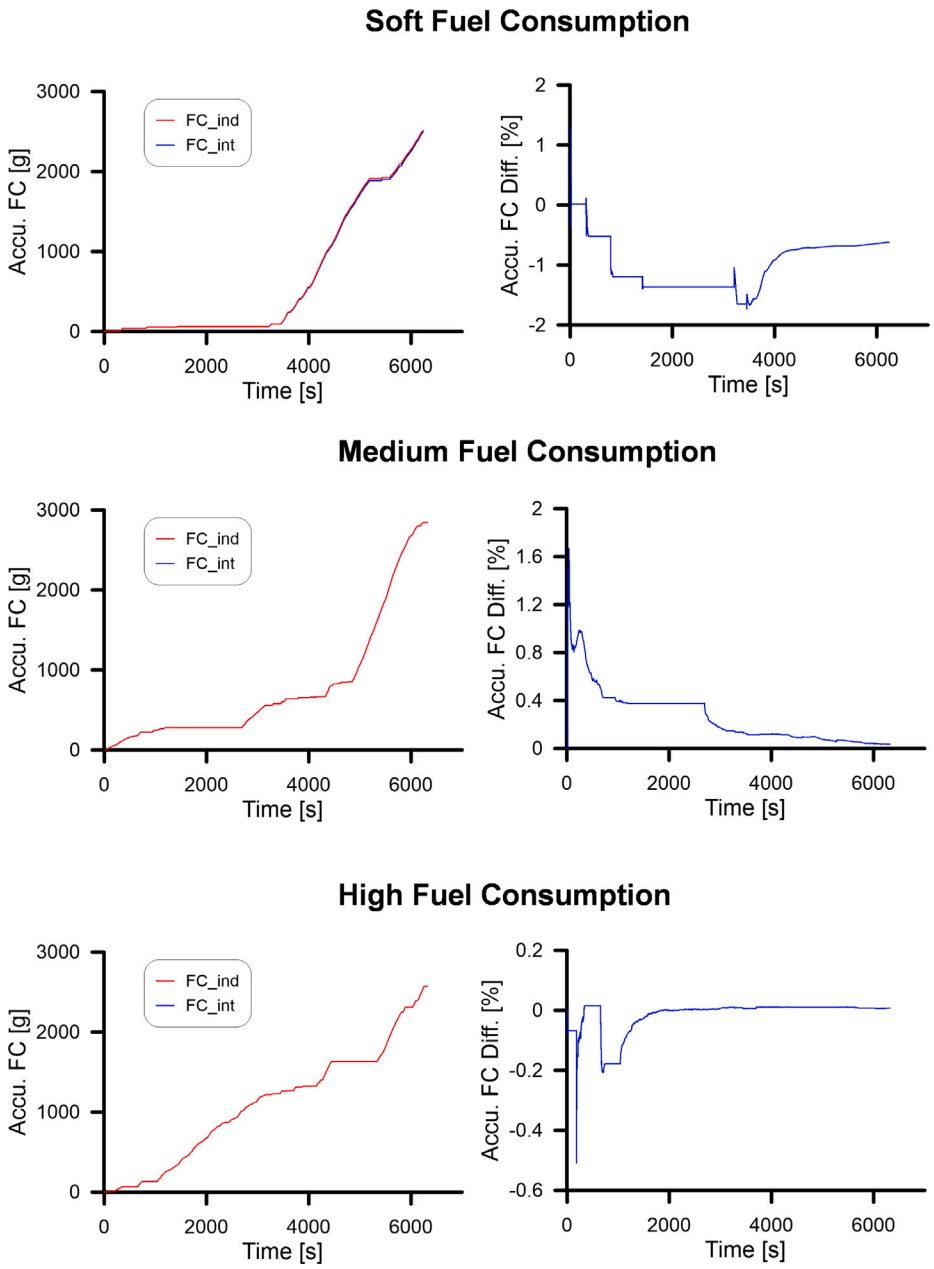

Fig. 18. Accumulated fuel consumption for warm conditions in RDE cycles where, in the legend, the *ind* indicates independent and *int* refers to integrated.

engine operating point according to the temperature of the coolant and the ECU signal. Once the adjustment process was finished, the validation of the three flows was performed for the rest of the engine map.

Fig. 11 shows a comparison between model results and experimental measurements of radiator coolant flows, in all the map and with different thermostat openings. The contour plots show a good agreement between predictions and experimental data which indicates that hydraulic resistances in all the elements have been well estimated. The error in radiator flow prediction is less than ±3% except in one operating condition, at which reaches 6.5% at 2500 rpm and 12 BMEP.

Overall, the model was considered to correctly predict the flows thorough the different branches in the coolant circuit for the whole engine map.

4.2.2. Thermal validation

For the validation of the hydraulic circuits' temperatures the heat rejected by both the engine and the turbocharger are required. With this purpose, the heat rejected used as input for the model was estimated by using the experimental measurements.

Once the flows are validated, the thermal fitting mostly depend on the heat exchanged in the different heat exchangers implemented in the hydraulic circuits. In the coolant circuit, the radiator, the cylinders, the turbocharger and the oil cooler are the elements that dissipate heat to the coolant. In the oil circuit, the turbocharger, the oil cooler and the cylinders are the elements dissipate heat to the oil. Among all the heat exchangers, the radiator and the oil cooler efficiency were used for fitting the temperatures in the circuits. However, to adjust the temperature drop in the different components, the proper heat had to be supplied to the system.

The procedure followed for adjusting and validating the thermal state has the following steps:

- Validate the coolant temperature drop of the engine with the measured heat flow.

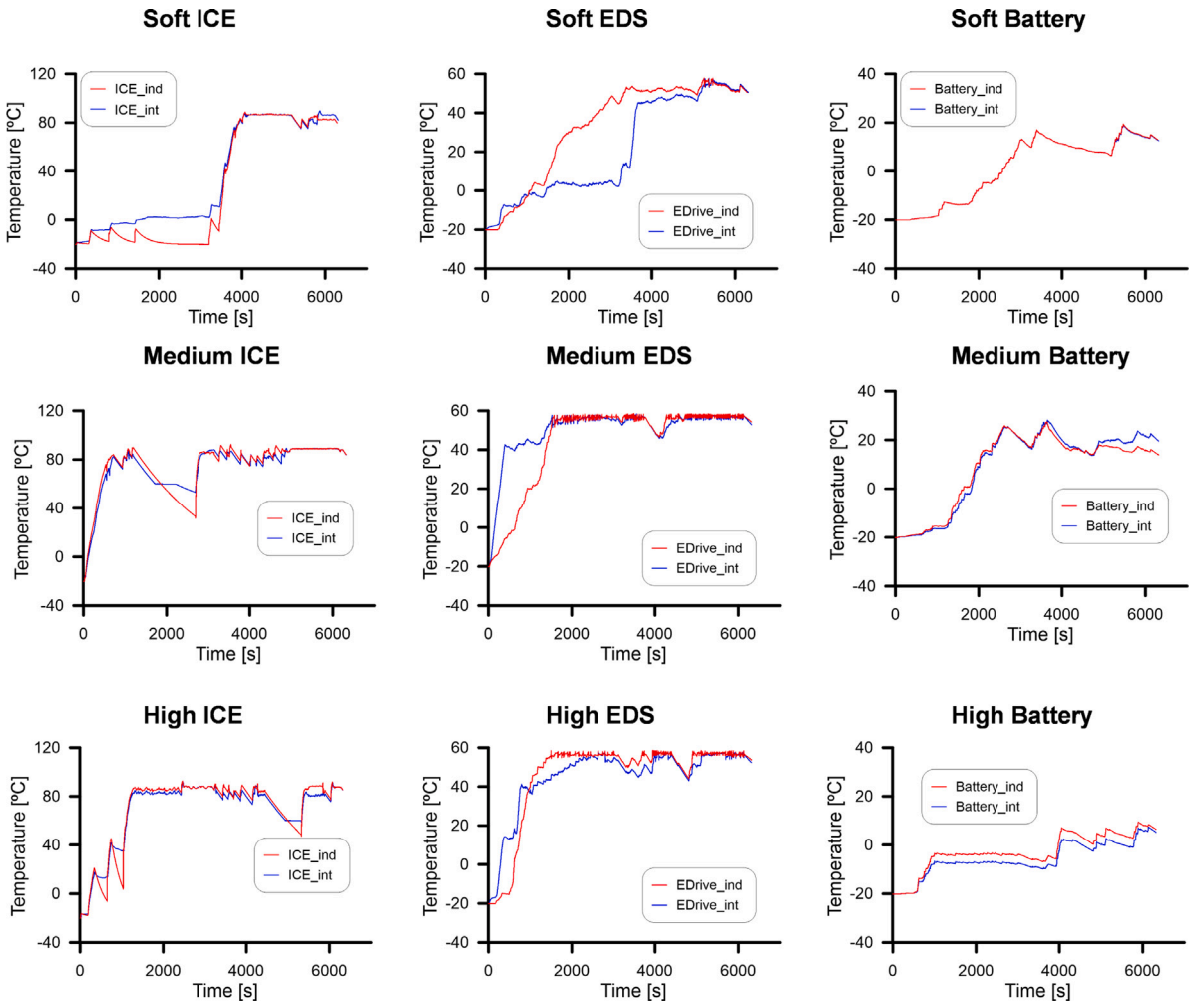

Fig. 19. ICE, battery and EDS temperature evolution for cold conditions in RDE cycles where, in the legend, the *ind* indicates independent and *int* refers to integrated.

- Adjust the engine inlet coolant temperature by modifying the heat rejected by the radiator.
- Validate the oil temperature by adjusting the oil cooler efficiency.
- Refine the heat rejected by the radiator.
- Validate the temperatures of different locations of the coolant circuit.

The heat rejected by the cylinders for each operating point was estimated with the experimental data and used as input in the cylinders (emulated with heat exchangers) of the coolant circuit. Coolant temperature drop showed a mean relative error around 0.9%. Plot (a) of Fig. 12 shows the comparison between the predicted and measured coolant temperatures at the inlet of the engine. The evaluation of the reliability of the model for predicting the oil temperature is presented in the plot (b) of Fig. 12. In both circuits, the observed errors demonstrated the capability of the model.

4.3. Transient conditions

To validate the coupling among the ICE main sub-models in transient conditions, three different RDE (Real Driving Emission) cycles were simulated. These cycles were defined by the control model. The considered cycles are soft, medium, and high (aggressive) cycle depending on their acceleration aggressiveness. The three cycles comply the limits established by the standards. These cycles were defined using a drive cycle generator developed in the work presented in Ref. [46]. This generator has been developed to synthesize cycles complying all the regulatory requirements of the real drive emission testing.

4.3.1. ICE transient validation

During transient simulations, the same 1D engine model is run, changing the engine speed and torque requested cycle-by-cycle. The engine speed is imposed to the model, while the torque request is targeted with an internal PID controller. All the information regarding the engine operating parameters, such as spark advance, valve timing and target boost pressure are interpolated according to the engine speed/torque map introduced in the steady state model. This approach allows to include a fully physical transient model of the GDI engine in the vehicle simulation.

Fig. 13 shows the comparison between predicted by the model (coupling of ICE Lumped Thermal Model, ICE Thermo-Fluid Dynamic Model and ICE Thermohydraulic Model) and measured engine speed and torque evolution of ICE during the three different RDE cycles defined before. The very good concordance between these two engine parameters is remarkable for the three cycles.

Fig. 14 shows the comparison between the measured and calculated coolant temperature at the inlet of the engine. In general, a good collapse of these results can be observed for the three cycles. Although the coolant temperature shows some discrepancy between 1000 s and 2800 s in the medium RDE cycle, the overall accuracy can be considered acceptable since the temperature rise and drop during starts and stops of the engine were correctly predicted by the model during all cycles. The comparison between the measured and predicted volumetric flow rate of the coolant through the oil cooler branch is presented in Fig. 14. These results show the remarkable capacity of the co-simulation tool to predict the coolant flow evolution at RDE cycles operation.

In Fig. 14 the oil temperature evolution is presented for the RDE cycles. In the soft cycle, it is observed that the model slightly overestimates the temperature during the first 1200 s. Additionally, after 5750 s the model underestimates the temperature because the coolant temperature is also underestimated by the model in that period. The same behaviour is observed for the last part of the medium cycle. Overall, the model was considered able to predict the trend of the oil temperature with good accuracy.

5. Simulations and results

In this section the main results obtained from the simulations of both the independent and integrated thermal management systems are presented. These thermal management systems were studied by means of a co-simulation of the ICE, Battery and EDS submodels as it can be observed in the scheme presented in Fig. 15. Three RDE cycles were selected to evaluate the impact on operating temperature and fuel consumption of the integrated thermal management strategies.

Fig. 16 shows the power required from each powertrain component during the RDE cycles. On one hand, when the battery power is positive, the battery pack is supplying energy (that is, in discharging mode) and when this power is negative, the battery pack is in charging mode. On the other hand, the EDS power is positive when it works as a motor and negative when it works as a generator. As explained before, the powertrain control strategy of the vehicle was defined to keep the state of charge of the battery along the cycle and to save the fuel consumed by the ICE. The simulations were launched for both warm (20 °C) and cold (−20 °C) conditions.

5.1. Warm conditions (20 °C)

In Fig. 17 the evolution of the calculated coolant temperatures of each powertrain component with the two TMS considered during the RDE cycles at warm conditions (ambient temperature at 20 °C) are shown.

With the integrated TMS configuration the temperature drops of the ICE coolant when the powertrain switches to electric mode (ICE stops) are avoided during the RDE soft cycle. During the first phase of the cycle (up to almost 4000 s) the ICE coolant temperature rises even when the engine stops due to the heat rejected by the EDS. Additionally, the integrated TMS maintains the coolant temperature above 40 °C around 77.3% of the total cycle time while in the independent TMS it is less than 46% of the total. It is important to take into account that, the higher the coolant temperature the higher the oil temperature because of the ICE oil cooler. For the case of the EDS in the soft cycle, the integrated TMS keeps the coolant temperature above 50 °C during 3035 s (a 48.0% of the total RDE cycle) while the independent TMS maintains the coolant temperature above 50 °C during 4770 s (a 75.8% of the total RDE cycle). In other words, a slower warm-up of the EDS is produced because of the heat exchanged between the ICE and EDS system in the first phase of the cycle. Although this could slightly increase the friction losses in the EDS, the lower temperature would directly increase the machine life time by reducing its thermal ageing [37].

A similar behaviour is observed in the high cycle during the first 1500 s. The integrated TMS reduced the ICE cooling during the second turn off of the engine. Additionally, the EDS warm up is reduced thanks to the heat evacuated from the ICE TMS. In this case, the battery temperature is slightly higher because of the head rejected from the EDS TMS.

Contrary to the previous cycles, the integrated TMS during the medium cycle presented limited benefit due to the nature of the cycle. From the beginning, the ICE is turned on till it reaches optimum temperature (thermostat opening). Benefits were observed during the long period (between 1000 s and 2600 s) in which the ICE is turned off. Once the temperature was close to 60 °C, it was possible to use the energy available at the EDS system. Therefore, an exchange of gains is observed for this cycle. ICE warming is slightly delayed at the cost of a significant reduction in EDS warming. In other words, the control strategy was already optimum from the ICE thermal state.

In Fig. 18 both the ICE accumulated fuel consumption for the integrated and individual TMS and their relative difference are presented. A negative value means that the integrated TMS decreases fuel consumption compared to the base case. Note that the more fuel is consumed during the cycle, the less relative gain is obtained because it gets diluted during the period time in which the ICE reached thermal stability (thermostat opened). For the soft cycle, the results show fuel savings around 0.62% with the integrated TMS. However, the gain is much more significant if it is only analysed till the ICE reached thermal stability. A 1.74% of fuel savings were obtained during this period of the soft cycle. As it was predicted in the temperatures evolution (Fig. 17), there were also fuel gains during the ICE warming up in the high cycle. When the ICE turns on (around 180 s) there is 0.5% of fuel saving due to the overheat absorbed from the EDS. However, the gain slightly decreased during the following 250 s in which the ICE TMS is rejecting heat to the EDS. The fuel saving immediately increase again till 0.2% when the ICE cooling is avoided when ICE turns off (between 600 s and 1100 s). Finally, the gain is diluted with time one the engine works in optimal temperature. In the case of the medium cycle, the ICE turns on from the beginning and it does not stop till it has reached optimal temperature. This explains why in the central plots of Fig. 18, the integrated TMS actually increases the fuel consumption till 1.6% because it slows down the warming up of the engine while the temperature of the ICE is below 60 °C. Nevertheless, this contributes to fasten the warming up of the EDS as it was observed in Fig. 17. However, when ICE turns off between 1000 s and 2700 s the integrated system avoid the ICE temperature drop which produces an improvement in the fuel consumption (0.2%).

From the energy management point of view, the medium cycle has the most optimal control strategy to avoid using the ICE out of its optimum operating temperature as it happened in first half of the soft cycle.

The integrated TMS could perfectly reduce the fuel consumption if a more sophisticated TM control is applied to the system. Setting a heating priority among the different subsystems could be a good solution. For the medium and high cycle, the actuated valve could be controlled in a way that only lets heat exchange when ICE coolant temperature is below the thermal flow of the EDS. However, this would add a level of complexity to the system. As it was stated before, the nature of the proposed ITMS was to develop a simple and robust system.

This was because increasing the coolant temperature directly rises the cylinder wall temperatures improving the combustion process. Furthermore, it also contributes to increase the oil temperature, which reduces the oil viscosity and, hence, a reduction of friction losses is produced when the temperature drops at the beginning of the cycle are avoided. The more time the ICE is operated at higher temperatures, the better its overall efficiency.

Although a potential temperature increment was expected in the exhaust gas, no significant impact was observed in the inlet (T3) and outlet (T4) temperatures of the turbocharger with the integrated thermal management system.

5.2. Cold conditions (−20 °C)

In Fig. 19 the coolant temperature evolution of ICE, EDS and Battery during the RDE cycles at cold conditions are shown. For all three cycles, the trends observed are very similar to the warm case, the ICE coolant temperature drops are avoided, and the EDS warming up slows down with the integrated TMS concept of the soft cycle and increases for the medium cycle. The temperature of the battery coolant does not change because the threshold temperature for cooling start in the EDS is not achieved till the very end of the cycle.

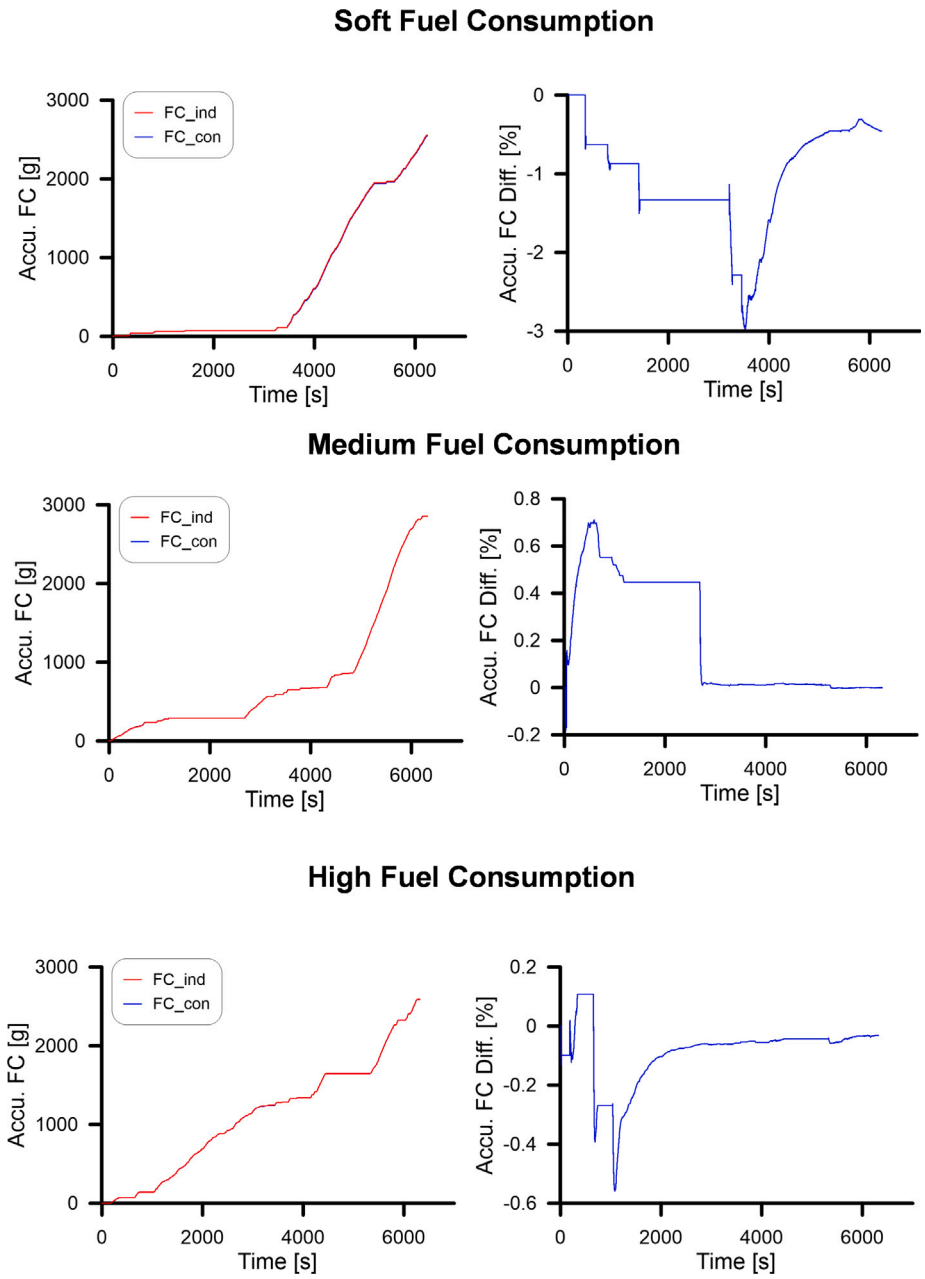

Fig. 20. Accumulated fuel consumption for cold conditions in RDE cycles where, in the legend, the *ind* indicates independent and *int* refers to integrated.

Finally, Fig. 20 shows that the accumulated fuel consumption decreases almost a 3% for the integrated TMS layout in the soft cycle. Almost double when compared with the warm case. This is because the friction losses reduction is even more significant at lower temperatures. For the medium cycle, as it happened in the warm case, the integrated TMS presented increased fuel consumption during the ICE warming time. However, this is much lower than the ambient case. Furthermore, the fuel saving during the ICE turning on after the long stop (between 1000 s and 2700 s) is much higher, reaching a 0.45%. Finally, for the high cycle, the maximum fuel savings with the ITMS were 0.55% during the ICE warming up. As it was stated before, the ITMS could improve the fuel saving by introducing new control algorithms.

6. Conclusions

The main conclusions of the work performed can be summarized as follows:

A novel methodology for studying integrated thermal management systems in hybrid vehicles have been developed and validated with the support of an extensive experimental campaign performed in a 1L GDI engine designed for hybrid vehicle powertrain. Both stationary and transient RDE cycles were launched in the testbench for validating the ICE implemented submodels. The coupling of models, which have been developed and calibrated in established modelling tools, has been successfully performed benefiting from their intrinsic capabilities using the standard FMU for co-simulation. The reliability of the model implemented for predicting the thermal management of the engine has been evaluated and the obtained discrepancies were within the order of magnitude of the measurement uncertainties. Different TMSs have been designed and simulated to evaluate the thermal flows in the hybrid vehicle. The approach for designing the ITMS considered the minimization of number of components and fulfilled thermal requirements of the different components of the hybrid powertrain.

The simulation results showed that an integrated TMS allows to avoid the temperature drop of the ICE coolant when the powertrain

switches to electric mode. Additionally, the accumulated fuel consumption decreased a 1.74% and 3% with the integrated TMS during the ICE warming up for the RDE soft cycle at 20 °C and −20 °C, respectively. Additionally, the maximum fuel saving were around 0.55% for the high cycle for both warm and cold conditions. Finally, for the case of the medium cycle, the integrated TMS proved to increase the fuel consumption during the ICE warming up time while reducing the warm up time of the EDS. Only when the ICE temperature was below the EDS optimum operating temperature, the integrated proved to be beneficial regarding duel savings.

Declaration of competing interest

The authors declare that they have no known competing financial interests or personal relationships that could have appeared to influence the work reported in this paper.

Data availability

The data that has been used is confidential.

Acknowledgements

Authors would like to sincerely acknowledge the founding support provided by Consellería de Innovación, Universidades, Ciencia y Sociedad Digital in the framework of the Ayuda Predoctoral GVA. (ACIF/2020/234).

References

[1] S.F. Tie, C.W. Tan, A review of energy sources and energy management system in electric vehicles, Renew. Sustain. Energy Rev. 20 (2013) 82–102, http://dx.doi.org/10.1016/j.rser.2012.11.077.

[2] R. Yuan, T. Fletcher, A. Ahmedov, N. Kalantzis, A. Pezouvanis, N. Dutta, A. Watson, K. Ebrahimi, Modelling and Co-simulation of hybrid vehicles: A thermal management perspective, Appl. Therm. Eng. 180 (May) (2020) 115883, http://dx.doi.org/10.1016/j.applthermaleng.2020.115883.

[3] G. Kalghatgi, Is it really the end of internal combustion engines and petroleum in transport? Appl. Energy 225 (May) (2018) 965–974, http://dx.doi.org/10.1016/j.apenergy.2018.05.076.

[4] F. Sher, S. Chen, A. Raza, T. Rasheed, O. Razmkhah, T. Rashid, P.M. Rafi-ul Shan, B. Erten, Novel strategies to reduce engine emissions and improve energy efficiency in hybrid vehicles, Clean. Eng. Technol. 2 (November 2020) (2021) 100074, http://dx.doi.org/10.1016/j.clet.2021.100074.

[5] Z. Liu, J. Song, J. Kubal, N. Susarla, K.W. Knehr, E. Islam, P. Nelson, S. Ahmed, Comparing total cost of ownership of battery electric vehicles and internal combustion engine vehicles, Energy Policy 158 (2021) 112564, http://dx.doi.org/10.1016/j.enpol.2021.112564.

[6] S. Bai, C. Liu, Overview of energy harvesting and emission reduction technologies in hybrid electric vehicles, Renew. Sustain. Energy Rev. 147 (April) (2021) http://dx.doi.org/10.1016/j.rser.2021.111188.

[7] R. Cipollone, D. Di Battista, A. Gualtieri, Head and block split cooling in ICE, in: IFAC Proceedings Volumes (IFAC-PapersOnline), 2012, http://dx.doi.org/10.3182/20121023-3-FR-4025.00056.

[8] A. Broatch, P. Olmeda, J. Martin, A. Dreif, Numerical study of the maximum impact on engine efficiency when insulating the engine exhaust manifold and ports during steady and transient conditions, SAE Int. J. Adv. Curr. Pract. Mobil. 3 (1) (2020) 661–671, http://dx.doi.org/10.4271/2020-37-0002.

[9] F.J. Arnau, J. Martín, P. Piqueras, Á. Auñón, Effect of the exhaust thermal insulation on the engine efficiency and the exhaust temperature under transient conditions, Int. J. Engine Res. 22 (9) (2021) 2869–2883, http://dx.doi.org/10.1177/1468087420961206.

[10] A.J. Torregrosa, A. Broatch, P. Olmeda, A. Dreif, Assessment of the improvement of internal combustion engines cooling system using nanofluids and nanoencapsulated phase change materials, Int. J. Engine Res. 22 (6) (2021) 1939–1957, http://dx.doi.org/10.1177/1468087420917494, arXiv:https://doi.org/10.1177/1468087420917494.

[11] T.M. Bandhauer, S. Garimella, T.F. Fuller, A critical review of thermal issues in lithium-ion batteries, J. Electrochem. Soc. 158 (3) (2011) R1, http://dx.doi.org/10.1149/1.3515880.

[12] J. Kim, J. Oh, H. Lee, Review on battery thermal management system for electric vehicles, Appl. Therm. Eng. 149 (November 2018) (2019) 192–212, http://dx.doi.org/10.1016/j.applthermaleng.2018.12.020.

[13] H. Chen, T. Zhang, Q. Gao, Z. Han, Y. Xu, K. Yang, X. Xu, X. Liu, Advance and prospect of power battery thermal management based on phase change and boiling heat transfer, J. Energy Storage 53 (2022) 105254, http://dx.doi.org/10.1016/j.est.2022.105254.

[14] T. Zhang, Q. Gao, G. Wang, Y. Gu, Y. Wang, W. Bao, D. Zhang, Investigation on the promotion of temperature uniformity for the designed battery pack with liquid flow in cooling process, Appl. Therm. Eng. 116 (2017) 655–662, http://dx.doi.org/10.1016/j.applthermaleng.2017.01.069.

[15] T. Zhang, C. Gao, Q. Gao, G. Wang, M. Liu, Y. Guo, C. Xiao, Y. Yan, Status and development of electric vehicle integrated thermal management from BTM to HVAC, Appl. Therm. Eng. 88 (2015) 398–409, http://dx.doi.org/10.1016/j.applthermaleng.2015.02.001, Special Issue for International Heat Transfer Symposium 2014.

[16] E. Gundabattini, R. Kuppan, D.G. Solomon, A. Kalam, D.P. Kothari, R. Abu Bakar, A review on methods of finding losses and cooling methods to increase efficiency of electric machines, Ain Shams Eng. J. 12 (1) (2021) 497–505, http://dx.doi.org/10.1016/j.asej.2020.08.014.

[17] G.D. Demetriades, H.Z. De La Parra, E. Andersson, H. Olsson, A real-time thermal model of a permanent-magnet synchronous motor, IEEE Trans. Power Electron. 25 (2) (2010) 463–474, http://dx.doi.org/10.1109/TPEL.2009.2027905.

[18] E. Agamloh, A. von Jouanne, A. Yokochi, An overview of electric machine trends in modern electric vehicles, Machines 8 (2) (2020) http://dx.doi.org/10.3390/MACHINES8020020.

[19] H. Fathabadi, High thermal performance lithium-ion battery pack including hybrid active-passive thermal management system for using in hybrid/electric vehicles, Energy 70 (2014) 529–538, http://dx.doi.org/10.1016/j.energy.2014.04.046.

[20] T. Kiss, J. Lustbader, D. Leighton, Modeling of an electric vehicle thermal management system in MATLAB/simulink, SAE Tech. Pap. 2015-April (April) (2015) 21–23, http://dx.doi.org/10.4271/2015-01-1708.

[21] T. Rana, Y. Yamamoto, Universal electric vehicle thermal management system, SAE Tech. Pap. 2020-August (August) (2020) 604–613, http://dx.doi.org/10.4271/2020-28-0002.

[22] C. Kaufmann, J. Frochte, A case study on fmu as co-simulation exchange format for fem models, 2016.

[23] P. Lu, Q. Gao, Y. Wang, The simulation methods based on 1D/3D collaborative computing for the vehicle integrated thermal management, Appl. Therm. Eng. 104 (2016) 42–53, http://dx.doi.org/10.1016/j.applthermaleng.2016.05.047.

[24] P. Casoli, A. Gambarotta, N. Pompini, L. Riccò, Development and application of co-simulation and "control- oriented" modeling in the improvement of performance and energy saving of mobile machinery, Energy Procedia 45 (2014) 849–858, http://dx.doi.org/10.1016/j.egypro.2014.01.090.

[25] A. Picarelli, V. Avila, S.P. Robinson, Thermal management strategies for integrated hybrid vehicle subsystems, in: 6th Hybrid and Electric Vehicles Conference (HEVC 2016), 2016, pp. 1–6, http://dx.doi.org/10.1049/cp.2016.0975.

[26] M. Cao, I. Kovent, J. Ku, Efficient thermal modeling and integrated control strategy of powertrain for a parallel hybrid EcoCAR2 competition vehicle, SAE Tech. Pap. 1 (2014) http://dx.doi.org/10.4271/2014-01-1927.

[27] K. G, K. C, Principal aspects and simulation of a hybrid demonstrator vehicle's cooling system, SAE Tech. Pap. 2007-January (August) (2007) 10, http://dx.doi.org/10.4271/2007-01-3483.

[28] T.J. Shelly, J.A. Weibel, D. Ziviani, E.A. Groll, Comparative analysis of battery electric vehicle thermal management systems under long-range drive cycles, Appl. Therm. Eng. 198 (2021) 117506, http://dx.doi.org/10.1016/j.applthermaleng.2021.117506.

[29] S. Lei, S. Xin, S. Liu, Separate and integrated thermal management solutions for electric vehicles: A review, J. Power Sources 550 (2022) 232133, http://dx.doi.org/10.1016/j.jpowsour.2022.232133.

[30] A. Lajunen, Y. Yang, A. Emadi, Recent developments in thermal management of electrified powertrains, IEEE Trans. Veh. Technol. 67 (12) (2018) 11486–11499, http://dx.doi.org/10.1109/TVT.2018.2876315.

[31] J. Ma, Y. Sun, S. Zhang, J. Li, S. Li, Experimental study on the performance of vehicle integrated thermal management system for pure electric vehicles, Energy Convers. Manage. 253 (2022) 115183, http://dx.doi.org/10.1016/j.enconman.2021.115183.

[32] S. Hemmati, N. Doshi, D. Hanover, C. Morgan, M. Shahbakhti, Integrated cabin heating and powertrain thermal energy management for a connected hybrid electric vehicle, Appl. Energy 283 (2021) 116353, http://dx.doi.org/10.1016/j.apenergy.2020.116353.

[33] M. Shams-Zahraei, A.Z. Kouzani, S. Kutter, B. Bäker, Integrated thermal and energy management of plug-in hybrid electric vehicles, J. Power Sources 216 (2012) 237–248, http://dx.doi.org/10.1016/j.jpowsour.2012.05.055.

[34] A. Marinoni, M. Tamborski, T. Cerri, G. Montenegro, G. D'errico, A. Onorati, E. Piatti, E.E. Pisoni, 0D/1D thermo-fluid dynamic modeling tools for the simulation of driving cycles and the optimization of Ic engine performances and emissions, Appl. Sci. (Switzerland) 11 (17) (2021) 1–21, http://dx.doi.org/10.3390/app11178125.

[35] J. Martin, F. Arnau, P. Piqueras, A. Auñon, Development of an Integrated Virtual Engine Model to Simulate New Standard Testing Cycles, SAE Technical Paper 2018-01-1413, 2018, http://dx.doi.org/10.4271/2018-01-1413.

[36] A. Broatch, P. Olmeda, J. Martin, J. Salvador-Iborra, Development and Validation of a Submodel for Thermal Exchanges in the Hydraulic Circuits of a Global Engine Model, SAE Technical Paper 2018-01-0160, 2018, pp. 1–10, http://dx.doi.org/10.4271/2018-01-0160.

[37] X. Wang, B. Li, D. Gerada, K. Huang, I. Stone, S. Worrall, Y. Yan, A critical review on thermal management technologies for motors in electric cars, Appl. Therm. Eng. 201 (2022) 117758, http://dx.doi.org/10.1016/j.applthermaleng.2021.117758.

[38] A. Broatch, P. Olmeda, X. Margot, L. Agizza, A generalized methodology for lithium-ion cells characterization and lumped electro-thermal modelling, Appl. Therm. Eng. 217 (2022) 119174, http://dx.doi.org/10.1016/j.applthermaleng.2022.119174.

[39] G. Montenegro, A. Onorati, G. D'Errico, T. Cerri, A. Marinoni, V. Tziolas, N. Zingopis, Prediction of driving cycles by means of a co-simulation framework for the evaluation of ic engine tailpipe emissions, SAE Tech. Pap. (June) (2020) 13, http://dx.doi.org/10.4271/2020-37-0011.

[40] L. Gascón, J.M. Corberán, Construction of second-order TVD schemes for non-homogeneous hyperbolic conservation laws, J. Comput. Phys. 172 (1) (2001) 261–297, http://dx.doi.org/10.1006/jcph.2001.6823.

[41] R.S. Benson, J.H. Horlock, D.E. Winterbone, The Thermodynamics and Gas Dynamics of Internal-Combustion Engines, Oxford science publications, Clarendon Press, 1982, v. 1.

[42] A. Pirooz, J. Van Mierlo, M. Berecibar, 3D thermal and 1D electro-thermal model coupling framework for lithium-ion battery cells in automotive industry platforms, in: 2021 IEEE Vehicle Power and Propulsion Conference (VPPC), 2021, pp. 1–6, http://dx.doi.org/10.1109/VPPC53923.2021.9699116.

[43] A. Arcila, X. Marcelle, Study of Conjugate Heat Transfer in Battery Cooling Systems for xEV Applications (Master's thesis), Universitat Politècnica de Valencia, 2021.

[44] F. Payri, J. Martín, F.J. Arnau, S. Artham, Analysis of temperature and altitude effects on the Global Energy Balance during WLTC, Int. J. Engine Res. 23 (11) (2022) 1831–1849, http://dx.doi.org/10.1177/14680874211034292, arXiv:https://doi.org/10.1177/14680874211034292.

[45] A. Broatch, P. Olmeda, A. García, J. Salvador-Iborra, A. Warey, Impact of swirl on in-cylinder heat transfer in a light-duty diesel engine, Energy 119 (2017) 1010–1023, http://dx.doi.org/10.1016/j.energy.2016.11.040, URL https://www.sciencedirect.com/science/article/pii/S0360544216316450.

[46] J.M. Luján, C. Guardiola, B. Pla, V. Pandey, Impact of driving dynamics in RDE test on NOx emissions dispersion, Proc. Inst. Mech. Eng. D 234 (6) (2020) 1770–1778, http://dx.doi.org/10.1177/0954407019881581, arXiv:https://doi.org/10.1177/0954407019881581.